2014

Mesoporous Tio2 Encapsulated Monometallic (Cu, Co, Ni, Pd, Sn, Zn) Nanocatalysts For Steam Reforming Of Methanol

Sri Lanka Owen
North Carolina Agricultural and Technical State University

Mesoporous TiO_2 Encapsulated Monometallic (Cu, Co, Ni, Pd, Sn, Zn) Nanocatalysts for Steam Reforming of Methanol

Sri Lanka S. Owen

North Carolina Agricultural & Technical State University

A thesis submitted to the graduate faculty

in partial fulfillment of the requirements for the degree of

MASTER OF SCIENCE

Department: Chemistry

Major: Chemistry

Major Professor: Dr. Debasish Kuila

Greensboro, North Carolina

2014

The Graduate School
North Carolina Agricultural and Technical State University
This is to certify that the Master's Thesis of

Sri Lanka S. Owen

has met the thesis requirements of
North Carolina Agricultural and Technical State University

Greensboro, North Carolina
2014

Approved by:

Dr. Debasish Kuila Major Professor	Dr. Zerihun Assefa Committee Member
Dr. Shamsuddin Ilias Committee Member	Dr. Margaret Kanipes-Spinks Department Chair

Dr. Sanjiv Sarin
Dean, The Graduate School

Biographical Sketch

Sri Lanka S. Owen was born March 18, 1990, in Fayetteville, North Carolina. She graduated from Seventy-First High School in 2008. She received her Bachelor of Science in Chemistry degree from Winston-Salem State University in 2012. In the fall of 2012, she was accepted to North Carolina Agricultural and Technical State University to pursue a Master of Science in Chemistry.

Dedication

This thesis is dedicated to Ora Owen, Linda Owen, Gary Davis, Joseph Flood, Saadia Owen, and Wayne Crowell with much love.

Acknowledgements

First I would like to thank God, because through him all things are possible. My gratitude goes to my advisor Dr. Kuila for allowing me to become a member of his research group and standing behind me firmly to reach my goals. I want to give special thanks to my committee members, Dr. Ilias and Dr. Assefa. A special appreciation goes to Dr. Deshmane who helped me so much throughout my research and I cannot give enough thanks. I am also thankful for Richard Abrokwah, William Dade, and Sara Al-Salihi who have helped me through early morning and late nights in the lab. I would like to thank Mr. James King (Chemistry Department) for his support in the experimental work and Mr. Bryce Holmes (School of Agriculture and Environmental Sciences) for his help with ICP analysis. I also thank the Department of Chemistry (NCAT) faculty, staff, and students for their support. This project was supported by the National Science Foundation (NSF) for the NSF-CREST Bioenergy Center (Grant No. HRD-124215).

Table of Contents

List of Figures

List of Tables

Abbreviations

Ar	Argon
BET	brunauer-emmett-teller
cm	centimeter
cmc	critical micellar concentration
CTAB	cetyltrimethylammonium bromide
CVD	chemical evaporation deposition
EISA	evaporation-induced self-assembly
FID	flame ionization detector
FTIR	fourier transform infrared spectroscopy
g	gram
GC	gas chromatography
h	hour
HF	hydrofluoric acid
HNO_3	nitric acid
HR-TEM	high resolution-transmission electron microscopy
ICP-OES	inductively coupled plasma-optical electron microscope
K	Kelvin
KBr	potassium bromide
MCT	mercury-cadmium-telluride
min	minutes
mL	milliliters
mm	millimeters

nm	nanometers
PEMFC	proton exchange membrane fuel cell
ppm	parts per million
PSD	position sensitive detector
SRE	steam reforming of ethanol
SRM	steam reforming of methanol
SMSI	strong support metal interaction
TCD	thermal conductivity detector
TEM	transmission electron microscopy
TGA-DSC	thermo gravimetric analysis- differential scanning calorimetry
TIPR	titanium (IV) isopropoxide
TPR	temperature programmed reduction
WGS	water-gas shift
XRD	x-ray diffraction

Abstract

Hydrogen is a renewable, clean energy source considered to be promising for energy and environmental sustainability. Steam reforming of methanol (SRM) to produce H_2 is ideal for fuel cell applications. One of the challenges of SRM at high temperature is the CO formation that poisons the Pt electrode in proton exchange membrane fuel cell (PEMFC). In order to address this issue, development of novel catalysts is necessary that can be used for PEMFC applications. In this study, a one-pot procedure containing TiO_2 precursor, metal salt, and cetyltrimethylammonium bromide surfactant was used to synthesize monometallic (M: Cu, Co, Ni, Pd, Sn, and Zn) nanoparticles supported on mesoporous TiO_2. The catalysts were characterized using TGA-DSC, N_2 adsorption-desorption, XRD, ICP-OES, TEM, FTIR and TPR techniques. Catalysts possess high surface area in the range of 99-309 m^2/g, depending on the type of metal and its loading. TEM images show highly mesoporous TiO_2 with uniform dispersion of metal nanoparticles. The XRD studies confirmed the existence of catalytically active anatase phase and the nanoparticulate nature of TiO_2 crystallites. Hydrogen production via SRM using these catalysts was studied to investigate their activity and CO selectivity in the reaction temperature range of 150-350 °C. Comparative SRM studies of different M-TiO_2 catalysts were carried out with 10 wt% of metal loading. Results from SRM studies at 250 °C suggest that the activity of the monometallic catalysts followed the order of Pd>Ni>Co>Zn>Cu>Sn, whereas for the lower CO selectivity it was Zn>Co>Sn>Cu>Pd>Ni. The 10%Zn-TiO_2 catalyst showed the best results with CO selectivity of 1.19%, H_2 selectivity of 99.66%, and conversion of 82.4% at 350 °C reaction temperature. In addition, the effect of Zn loading from 5-20% was fully investigated on the activity and selectivity of the catalyst.

CHAPTER 1

Introduction

The rising environmental concerns associated with the rigorous use of fossil fuels for the production of energy and chemicals have gained much attention over the past century due to atmospheric pollution by greenhouse gases like CO_2, CO, and NO_x. With the availability of the fossil fuels diminishing and increasing environmental issues related to greenhouse gas emissions, the search for technology using renewable energy resources to overcome non-sustainable nature of current energy systems is essential to the economy [1]. Hydrogen has become promising as a fuel because it is clean, carbon-free, and can be readily converted to electrical energy to power fuel cell electric cars. [2].

Fuel cells have attracted much attention over the years as a potential device for energy transformation. They have high efficiency and low emission of pollutants, which makes them promising as future means of energy source [3]. However, there are several problems associated with the use hydrogen for fuel cells that include safety concerns, cost of transportation, storage and handling. These issues have led to the search for suitable energetic liquid fuels that can be used for hydrogen production [4].

Steam reforming is the catalytic hydrothermal conversion of hydrocarbons and alcohols to hydrogen with other by-products (CO and CH_4). A typical steam reforming reaction for alcohols can be generalized in equation 1.1.

$$R'OH + x\ H_2O \rightarrow y\ H_2 + CO_2 \qquad (1.1)$$

The alcohols generally used in steam reforming reactions are ethanol, methanol, and glycerol. The advantage of using methanol over other alcohols is that hydrogen can be produced at lower temperature (150-350 °C) making it more energy efficient and lesser cost of production. Other

advantages include high hydrogen-to-carbon ratio (4:1), a high yield of hydrogen on weight and volume, and the absence of the C-C bond leading to low tendency of soot formation. In contrast, steam reforming of ethanol and glycerol require higher temperatures (>500 °C) to produce hydrogen because of the presence of C-C bonds. Thus, methanol reforming has become more desirable and the development of highly active catalysts giving lower CO selectivity for steam reforming of methanol (SRM) has gained much interests in recent years [5].

The support of active components in catalysts plays a crucial role in the activity and stability of catalysts due to their unique interactions. Although a great deal of research has been done over past 30 years, the interactions between the support and the metals are still not well understood. There are several different metal oxides namely, alumina, silica, zirconia, ceria, and titania, which are commonly used as inorganic hosts of catalytically active components. An important property of the support material is a large specific surface area, in which the incorporated catalytically active phase can be highly dispersed. Mesoporous materials meet the requirements for the selection of a support due to their very high surface area allowing high dispersion of active sites and large pores to facilitate mass transfer [6]. Another interesting feature of mesoporous materials is their ability to modify the surface functionality, incorporate catalytic functions, and change the textural properties for applications, such as catalysis [7].

Non-silica based mesoporous materials have been synthesized over the past two decades. The preparation of the non-siliceous mesoporous materials began to gain much interest in the beginning of the 21st century [8]. With increased interests in non-siliceous supports, scientists began to prepare semi-crystalline, ordered, and ordered crystalline mesoporous materials using soft and hard templating methods [8]. The physical properties of these supports such as, their particle and pore sizes, specific surface area, and wall thickness can be altered by changing

hydrothermal conditions, surfactants, and calcination temperatures. Manipulations of the support are advantageous to mesoporous metal oxides because it allows controllable features in size and shape of the resulting particles.

One of the non-silica based mesoporous supports such as TiO_2 has been used extensively in photo-catalysis for photo-degradation of various pollutants. There have been many efforts to synthesize mesoporous titania with high surface area and apply them in many fields. Mesoporous titania is expected to play an important role in solving environmental and pollution issues [9]. It has also been used in steam reforming reactions for its unique interactions with metals. Other advantages of mesoporous titania include high surface area, uniform pore size, and accessible open framework when used as a catalyst support for steam reforming reactions.

The main objective of this thesis is to study the individual effect of different M-TiO_2 (where as, M= Cu, Co, Ni, Pd, Sn, and Zn) catalysts in the steam reforming of methanol (SRM) reactions. The main problem with catalysts in methanol steam reforming reactions at high temperature is the formation of CO, which poisons the Pt electrode in the PEMFC [10]. To overcome this issue, the development of novel catalysts with lower emission of CO is extremely important. Thus, the present study investigates the comparative effect of different metals incorporated in high surface area mesoporous TiO_2 support on SRM activity and CO selectivity due to their unique metal-support interactions. For the development and investigation of M-TiO_2 catalysts, this research will cover the following:

1. Synthesis of different M-TiO_2 catalysts with 10 wt% and Zn-TiO_2 with 5-20 wt% metal loading using a one pot procedure.
2. Detailed characterization using TGA-DSC, XRD, BET, ICP-OES, TEM, FTIR, and TPR techniques to study the physical and chemical properties of the catalysts.

3. Testing of the synthesized M-TiO_2 catalysts in the steam reforming of methanol (SRM) for H_2 production.

This thesis is divided into five chapters. This introductory chapter, CHAPTER 1, gives a brief background and the motivation behind this work. A literature review is presented in CHAPTER 2, which gives an overview on hydrogen as a fuel, its applications, and production, the steam reforming of alcohols, mesoporous materials, mesoporous titania and its synthesis, metals in mesoporous materials, and metals in mesoporous supports for steam reforming of methanol. CHAPTER 3 includes the materials and experimental procedure used to synthesize and characterize mesoporous TiO_2 and M-TiO_2, catalysts for steam reforming of methanol. The results and discussion of this study are presented in CHAPTER 4. Finally, conclusions and plans for future work are presented in CHAPTER 5.

CHAPTER 2

Literature Review

2.1 H_2 as a Fuel, Other Applications, and Its Production

Hydrogen has gained more interest in recent years since it has been forecasted to become the major source of energy in the future. Hydrogen is considered as a clean burning fuel that can be stored as a liquid and/or gas and can be used for transportation and stationary power generation when used as a fuel for the PEMFC. Hydrogen is used as a feedstock in the chemical, food, and refining industries and is required to meet the global needs of cleaner products. Refining industries are in high demand for hydrogen because of its use for desulfurization, hydrogen treating, and the production of chemicals [11]. Hydrogen is produced mostly from natural gas and oil, but contains high levels of carbon dioxide [12]. Hydrogen can also be produced from biomass conversion, electrolysis of water, and chemical hydrides [11].

The most economical way to produce hydrogen is from reforming of hydrocarbons. Reforming processes can be from steam (steam reforming), oxygen (partial oxidation), or the mixture of air and steam (auto thermal reforming). Steam reforming is more favorable because it yields higher hydrogen concentration than that obtained from partial oxidation and auto thermal reforming [10]. The development of suitable hydrogen production systems from renewable sources, such as steam reforming can help conquer the problems associated with green house gas emissions [12].

2.2 Steam Reforming of Alcohols

Alcohols have become promising candidates for H_2 production as several feedstocks are available and more significantly due to their ability to react with water (steam) to generate hydrogen at low temperature [13]. Steam reforming of alcohols that have been reported in

literature include methanol, ethanol, and glycerol. However, the latter alcohols require higher temperature for reforming because of their longer C-C chains. Thus, steam reforming of methanol has become more favorable due to its low cost, ability to reform at lower temperature, its high hydrogen to carbon ratio, and the absence of excessive by-products. Methanol is also considered a synthetic fuel that does not suffer from sulfur contamination, which is a big advantage to fuel reforming because the system does not need a front end desulfurization operation nor sulfur-tolerant catalyst to operate on methanol [5].

Steam reforming of methanol into gaseous mixtures can be described in equations 2.1-2.3. The reforming reaction shown in equation (2.1) is endothermic, as energy is required to run the reaction. Methanol reacts with water to produce carbon dioxide and 3 moles of hydrogen.

$$CH_3OH + H_2O \rightarrow CO_2 + 3H_2 \qquad \Delta H = 49.5 \text{ kJ mol}^{-1} \qquad (2.1)$$

$$CH_3OH \rightarrow CO + 2H_2 \qquad \Delta H = 90.6 \text{ kJ mol}^{-1} \qquad (2.2)$$

$$CO + H_2O \leftrightarrow CO_2 + H_2 \qquad \Delta H = -41.2 \text{ kJ mol}^{-1} \qquad (2.3)$$

However, this reaction is not clean and other products are formed that have to be taken into consideration [10]. SRM has two side reactions, methanol decomposition followed by the water-gas shift (WGS) reaction shown in equations 2.2 and 2.3, respectively. In equation (2.2), the decomposition of methanol takes place to produce carbon monoxide and 2 moles of hydrogen. Some of the carbon monoxide reacts with water in the reversible WGS reaction shown in equation (2.3) to produce carbon dioxide and hydrogen. Carbon monoxide is considered a by-product of SRM reactions and at higher concentration (>10 ppm) it can poison the Pt electrode of the PEMFCs [10]. Therefore, the WGS reaction is very important in converting the unwanted carbon monoxide into carbon dioxide. The development of novel active catalysts for steam

reforming reactions that can produce hydrogen with minimal CO is in high demand for the successful employment in PEMFCs. Mesoporous materials have been found advantageous as supports towards the development of novel active catalyst for steam reforming reactions. The advantages of using mesoporous materials in catalysis include, high surface area, which allows higher concentration of active sites per mass of the material and large pores that are available for mass transfer [6].

2.3 Mesoporous Materials

According to IUPAC definitions, porous materials have been divided into three categories; mircroporous (pore size <2 nm), mesoporous (2-50 nm), and macroporous (>50 nm). Mobil Oil Corporation scientists were the first to discover the features of novel type silica and its family of ordered M41S material. MCM-41, which stands for Mobile Composition of Matter No. 41, is the most studied mesoporous material that consists of hexagonal pores and a narrow pore size distribution [14]. Modification and optimization of the reaction conditions yielded highly ordered silicates and aluminosilicates, which sparked interest in synthesis and characterization of different related materials [6].

There have been many mesoporous metal oxides other than SiO_2 that includes ZrO_2, Al_2O_3, WO_3, CeO_2, SnO_2, and TiO_2. These mesoporous materials have advantages due to their ability to stabilize metal or metal oxide particles and halt the growth no larger than the pore size. Of these metal oxides, mesoporous titania has been extensively investigated for its electronic and optical properties [15] and it is a commonly used catalyst support due to its unique interaction with metal particles, uniform pore size, and open frameworks for mass transfer.

2.3.1 Mesoporous titania. Titania (TiO_2) is cheap, chemically stable, innocuous, environmental friendly and biocompatible, archaic material that is commonly used as a white

pigment in paints, cosmetics, and health care products for many years [15]. Recently, it has been found that titania is more useful for the sustainability of energy generation [15]. More specifically, mesoporous TiO_2 has gained much interest in photo-catalysis because of its stability, low cost, capability of decomposing contaminants in water and air purification, and device flexibility [16]. It has advantages such as large surface area, uniform pore size, and open framework for applications such as, photo-catalysis, solar cells, lithium ion batteries, sensors, and catalysts supports [17]. The surface area of mesoporous titania can range from ~ 89-700 m^2/g depending on the experimental approach used for its synthesis [15].

2.3.2 Synthetic approaches of mesoporous titania. There are two main procedures to synthesize mesoporous titania: i) sol-gel method and ii) hydrothermal method. A description of each synthesis is presented in this section.

In the 1960s, the sol-gel method was developed due to the need for new synthesis methods in nuclear industries [18]. Sol is considered a stable dispersion of colloidal particles or polymers in a solvent. The gel is a three dimensional continuous network, which encloses the liquid phase and the network is built from agglomeration of the colloidal particles. Inorganic precursors undergo hydrolysis and polycondensation reactions to form a colloid and a gel. A typical method consists of the mixture of metal alkoxides or salts in water or solvents, typically alcohols, at elevated temperatures [19]. The structure of solid phase is made from colloidal particles to a polymeric network gel. Drying and calcination of the sol-gel can lead to oxide particles with high surface area and controlled crystallinity [20].

Antonelli and Ying [21] were the first to report the synthesis of mesoporous titania, by a sol-gel process with a titanium isopropoxide precursor and alkylphosphate surfactant as the template. The material had hexagonal mesostructure and high stability when calcined at 350 °C.

However, a significant amount of phosphate remained in the sample after calcination. Phosphate surfactants limit the use of mesoporous titania as a catalyst support due to poisoning of the active site of the support. Antonelli et al. [22] also reported the synthesis of titania with a non-phosphated surfactant, using dodecylamine as the template, but the obtained material had poor thermal stability after calcination at 300 °C. The advantages of this method include enhancement of surface stability, improvement of homogeneity, surface area, and porosity of multi-component systems [23]. However, the disadvantages of the sol-gel method include high carbon content from the use of organic reagent during preparative step, long aging time (5-15 days), expensive metal alkoxides, and uncontrollable particle sizes [15].

The hydrothermal method includes crystallization techniques to obtain homogenous or heterogeneous phase reactions at high temperature and pressure in aqueous solutions. Surfactants are added to control the particle size and limit the agglomeration unlike the sol-gel process. The powders obtained are either amphorous or crystalline depending upon reaction conditions. High calcination temperatures are not required for this process, which is a major advantage [24]. Other advantages include controllable particle size by altering starting materials and reaction conditions. However, hydrolysis and polymerization of Ti precursors in aqueous solution are not easily controlled resulting in a decrease in high mesostructure regularity over a large domain [15].

In order to control the hydrolysis and polymerization of Ti precursors in aqueous solution, an evaporation-induced self-assembly (EISA) approach was developed by Brinker and co-workers. This approach begins with the homogenous solution of titania precursors and surfactant in ethanol/water solvent with $c_0 << CMC$ (critical micellar concentration). With the increase in surfactant concentration, the self-assembly of titania-surfactant micelles are able to

organize into ordered liquid-crystalline mesophases. The method provides the preparation of mesoporous materials in dilute non-aqueous medium, which controls the hydrolysis and polycondenstaion of the metal precursor [25]. The pore sizes of mesoporous titania depend upon the surfactant templates, in which catonic quaternary surfactants with long alkane chains can yield large pore sizes. Soler-Illia et al. [26] synthesized hexagonally ordered mesoporous TiO_2 using cetyltrimethylammonium bromide (CTAB), which is considered a catonic surfactant, through the EISA process. After that, the synthesis of mesoporous TiO_2 with various precursors, surfactants, and ratio of precursor to surfactant were used to yield different mesostructures and pore-wall parameters [15]. Gajjela et al. [27] reported the synthesis of mesoporous titania with the use of several catonic surfactants including CTAB. Different molar ratios of surfactant to precursors were compared for the materials using the EISA process.

Both sol-gel and hydrothermal methods are aimed to synthesize mesoporous titania. However, the hydrothermal method is more favorable due to its ability to control particle sizes, which is important in catalysis. The particle sizes can also be controlled with the addition of metals into mesoporous materials. Since ordered mesoporous supports are not often used as catalysts, the incorporation of active sites into the walls of the support or deposition of active species on the inner surface of material is utilized to improve the performance of catalysts [6].

2.4 Metals in Mesoporous Materials

Metal particles incorporated in different supports have been used in catalysis for many decades. The high dispersion of catalytically active particles in support materials is very important to catalysis. The use of ordered mesoporous materials with high surface areas and controllable pore sizes meet the requirements for high dispersion. There are several pathways for the deposition of the active metal compound onto the mesoporous support. Some of these

methods include chemical vapor deposition (CVD), impregnation, ion exchange, and one-pot synthesis.

2.4.1 Chemical vapor deposition (CVD). CVD is a process used to synthesize metal oxide nanoparticles with high purity and superior performance. This method consists of the deposition of solid material from a gaseous phase and is typically used in the semiconductor industry for micro-fabrication to produce thin-films. There are many CVD processes reported for the formation of nanoparticles, but the pore volume of the support limits the amount of metal loading. The substrate is first exposed to volatile precursors that react with substrate to produce the desired deposition. The nucleation and growth of the oxide nanoparticles follow solid-solid crystallization at higher temperature [24].

2.4.2 Ion exchange method. This technique involves the deposition of metal ions to the support by ion exchange. The negative charge of the pore walls exchanges charges with the cationic metal ions in aqueous solution. During reduction, some of the active sites are liberated, which allows the performance of the next exchange. The disadvantage of this method is its restricted amount of metal loading due to the capacity of the support and poor uniform distribution of the metal on the support [28].

2.4.3 Impregnation method. Impregnation also known as ‘wet chemistry’ is commonly used for the synthesis of supported metal catalysts, where the solid support is treated with a solution of metal precursor dissolved in a solvent to fill the pores and form a thick paste. The solvent is removed and the resulting solid is dried and calcined before catalyst testing. The support then undergoes deposition that will convert the metal precursor to an active species. These supports are considered thermally stable and can withstand the process of activation of these metal precursors, in which the catalyst are normally activated under a stream of hydrogen

gas at high temperature [24]. The major disadvantage of this method is the lack of uniform distribution of metal particles on the support, as they remain mainly in the pores [29].

2.4.4 One-pot synthesis. The one-pot synthesis has been reported by many researchers for the preparation of the metal and support simultaneously [30, 31]. The one-pot synthesis consists of the addition of metal precursors to the reactant solution and incorporating the metal during templated synthesis of the support. The preparation of mesoporous silica (MCM-41) containing palladium (Pd) nanoparticles by one-pot synthesis using a mixture of HCl-$PdCl_2$ in aqueous solution, cationic surfactant (CTAB), and silica source tetraethyl orthosilicate (TEOS) was reported by Wang et al. [32]. The PdO generated from the aqueous solution was capped by the CTA^+ surfactant micelle and interacted with anionic silicate species to form PdO/SiO_2 mesophase through templating [32]. This one pot synthesis is represented in Figure 2.1. When compared to the impregnation method, the one-pot method has been observed to yield uniform distribution of active sites [33]. This procedure eliminates pre-synthesis of the hard-template and post-synthesis treatments of mesoporous materials [34]. In this present work, the metal precursors and titania precursor are used in a one-pot procedure to obtain mesoporous titania supported catalyst.

2.5 Metals in Mesoporous Supports for Steam Reforming

Metal particles incorporated into mesoporous supports have a large surface to volume ratio compared to bulk material, which makes them attractive candidates for catalytic applications [35]. There are many studies found in literature on steam reforming with various supports and metals. Some of the metals used in steam reforming reactions include copper-based catalysts, group 8-10 metals (Ru, Rh, Pt, Pd, Ni, Co), and Zn/Sn-based catalyst.

2.5.1 Copper based catalysts. Copper-based (Cu) catalysts are extensively used in SRM reactions. Most studies on copper catalyst focus on the effect of the preparation method. Researchers have investigated the effect of preparation method and found that each step could affect the properties of the catalyst [36]. Liu et al. [37] reported active catalyst with higher values of copper dispersion and surface area with small particles. It has been reported in literature that CeO_2 has unique interactions as a support and that Cu/CeO_2 showed high activity due to highly dispersed Cu metal particles and unique interactions between Cu and CeO_2. However, copper catalyst are known for severe deactivation due to changes in oxidation state, sintering, or coke deposition [36]. Cu/ZnO systems have also been studied due to their ability to promote the low temperature water-gas shift reaction in the steam reforming of methanol. Cu-ZnO supported on Al_2O_3 were shown to deactivate at extended times on the stream and at higher temperatures, which made them not acceptable to fuel cell applications [13].

2.5.2 Group 8-10 metals. A researcher by the name of Iwasa sparked the study of group 8-10 metal-based catalysts by investigating the catalytic performance of these metals in the steam reforming of methanol [36]. Palladium (Pd) supported in ZnO is the most commonly catalyst studied in this group for the steam reforming of methanol. New approaches of using different supports that had higher surface area than ZnO were studied [4], but led to the study of Zn addition as a bi-metallic catalyst. Pd/ZnO catalyst reaction activity was effected by the supports applied and were reported to have high reaction selectivity [38]. It was later found that Pd/ZnO formed a Pd/Zn alloy confirmed by x-ray diffraction (XRD) and x-ray photoelectron spectroscopy (XPS) [39].

Nickel (Ni) catalysts are mainly reported in literature for the use of steam reforming of ethanol to produce hydrogen [13]. Transition metals, such as Ni are known to facilitate C-C bond

cleavage in reforming processes. Ni is also considered to be cheap and useful to industrial catalyst in hydrocarbon reaction, but they suffer from deactivation cause by the formation of coke [40]. Pérez-Hernández et al. [13] reported that Ni supported on mixed oxide CeO_2-ZrO_2 for the oxidative steam reforming of methanol were highly active and stable. High selectivity towards hydrogen was observed with Ni support on ZrO_2. However, the WGS reaction does not occur with this catalyst. Monometallic and bimetallic catalysts with Ni and Cu metal precursors supported on ZrO_2 were synthesized for the oxidative steam reforming of methanol. It was observed that Ni/ZrO_2 had higher catalytic activity than Cu/ZrO_2 [41].

Cobalt (Co) catalysts are mainly reported in literature for the steam reforming of ethanol [42]. Co-based catalysts have been studied over several supports, such as TiO_2, Al_2O_3, and ZrO_2 for the steam reforming of ethanol [43]. It was found that ethanol conversion could be correlated with metal dispersion of the Co metallic site when supported on TiO_2, Al_2O_3, and ZrO_2. The Co-ZrO_2 catalyst showed the highest metal dispersion and hydrogen yield compared to the other Co-supported catalyst. In another study, Batista et al. [44] found that Co supported on Al_2O_3 and SiO_2 mainly contained the oxide phase of Co_3O_4 confirmed by temperature programmed reduction (TPR) experiments. Both catalysts promoted the WGS reaction, but the Co/Al_2O_3 showed better removal of CO with complete conversion of ethanol and Co/SiO_2 exhibited better selectivity towards hydrogen.

2.5.3 Zinc and tin-based catalysts. There are studies on the use of Zinc (Zn) supported catalyst in steam reforming reactions. ZnO is normally used in combination with Cu or Pd as a catalyst support [45, 46]. Pinzari et al. [47] reported the use of Zn support on titania for the steam reforming of methanol and the combined reforming of methanol (SRM and partial oxidation of methanol). It was observed that the physico-chemical properties such as surface area,

crystallinity, and catalytic performance depended on the composition of the catalyst. The Zn/TiO_2 showed its highest catalytic activity at 400 °C in SRM reactions and that a proper amount of zinc was required to prevent coking and reduce the formation of by-products.

The use of other metals, such as tin (Sn) has also been considered for SRM. In literature, the influence of Sn addition to $Ni/MgO\text{-}Al_2O_3$ catalyst for steam reforming processes was studied in SRM reactions [40]. Sn was added to $Ni/MgO\text{-}Al_2O_3$ catalysts to promote bimetallic systems that could prevent the formation of nickel carbide and assist in the reduction of coke formation. However, it was observed that the addition of Sn decreased catalytic activity of SRM reaction. There is not much in literature on the use of monometallic Sn catalyst for steam reforming processes.

Commercially available and low surface area mesoporous titania is widely used in steam reforming studies. To the best our knowledge, there has not been any thorough investigation reported in the literature of different metals supported on high surface area mesoporous titania and their performance in SRM reactions. It is expected that high surface area mesoporous titania could decrease metal loading, increase the metal dispersion, and thereby eliminate deactivation of catalyst due to sintering. In this work, the properties of Ni, Cu, Co, Sn, Pd, and Zn supported on mesoporous titania, synthesized using a one-pot procedure, will be explored using different characterization techniques. The main goal is to investigate the performance of these $M\text{-}TiO_2$ catalysts in SRM reactions to address their unique strong metal-support interactions.

CHAPTER 3
Experimental Procedures

3.1 Chemicals

Table 3.1 shows a complete list of chemicals used in the present work. All chemicals were used without further purification. The distilled water used for all experiments was purified using Mill-Q Advantage A10 Elix 5 system obtained from Millipore Corporation (Bedford, MA, USA).

Table 3.1

List of Chemicals

Formula	Full Name	Manufacturer	Specification
$C_{16}H_{33}N(CH_3)_3Br$	Cetyltrimethylammonium bromide (CTAB)	Sigma-Aldrich	99%
$C_{12}H_{28}O_4Ti$	Titanium isopropoxide	Acros Organics	98%
$Ni(NO_3)_2 \cdot 6H_2O$	Nickel Nitrate hexahydrate	Fischer Scientific	-
$Cu(NO_3)_2 \cdot H_2O$	Copper nitrate hydrate	Sigma-Aldrich	98%
$CoCl_2 \cdot 6H_2O$	Cobalt chloride hexahydrate	Sigma-Aldrich	-
$Zn(NO_3)_2 \cdot 6H_2O$	Zinc nitrate hexahydrate	Sigma-Aldrich	98%
$SnCl_2 \cdot 2H_2O$	Tin chloride dihydrate	Sigma-Aldrich	98%
$Pd(NO_3)_2 \cdot H_2O$	Palladium nitrate hydrate	Sigma-Aldrich	-
NH_4OH	Ammonium hydroxide	Acros Organics	-
C_2H_5OH	Ethanol	Fischer Scientific	-
HF	Hydroflouric acid	Fischer Scientific	51%
HNO_3	Nitric acid	Fischer Scientific	68%
	Sand (white quartz)	Sigma-Aldrich	-

Table 3.1

Cont.

	Quartz wool	Fischer Scientific	-
KBr	Potassium bromide	Fischer Scientific	-

3.2 Synthesis

3.2.1 Mesoporous-TiO_2. Mesoporous titania was synthesized using the molar ratio of 1 TIPR: 0.52 CTAB: 282 H_2O: 26.21 ethanol. Initially, a water-ethanol solution with 4/1 (water/ethanol) volumetric ratio was prepared and to this solution a measured quantity of TIPR was added drop-wise very slowly with continuous vigorous stirring. The stirring was continued for another 30 min after TIPR addition. Then NH_4OH was added drop-wise until the pH was 10. The resulting mixture was stirred for 24 h at room temperature. The precipitate was washed with water until the pH of the filtrate was 7 and then with ethanol followed by filtration. The filtered material was air dried for ~24 h and then dried in an oven at 110 °C for 24 h. Finally, the dried material was calcined at 350 °C for 5 h with the heating and cooling rate of 2 °C/min to get the crystalline TiO_2.

3.2.2 One-pot synthesis of M/TiO_2. Mesoporous titania containing metal particles was synthesized using the molar ratio of 1 TIPR: 0.52 CTAB: 282 H_2O: 26.21 ethanol. The quantities of the metal precursors were used according to the metal loading requirement of the final catalyst. Initially, a water-ethanol solution with 4/1 (water/ethanol) volumetric ratios was prepared and to this solution measured quantity of CTAB was added and stirred for 30 min to get clear solution. In another beaker, a solution of metal salt in ethanol was prepared. After stirring for 30 min, this solution was mixed with CTAB solution and stirred again. To this solution measured quantity of TIPR was added very slowly and drop-wise with continuous vigorous

stirring. The stirring was continued for another 30 min after TIPR addition. Then NH_4OH is added drop-wise to adjust the pH ~ 10. The resulting mixture was stirred for 24 h at room temperature. The precipitate was washed with water to obtain the filtrate of pH 7 and then with ethanol and filtered. The filtered material was air dried for ~24 h and then dried in an oven at 110 °C for 24 h. Finally, the dried material was calcined at 350 °C for 5 h with the heating and cooling rate of 2 °C/min to get the crystalline TiO_2.

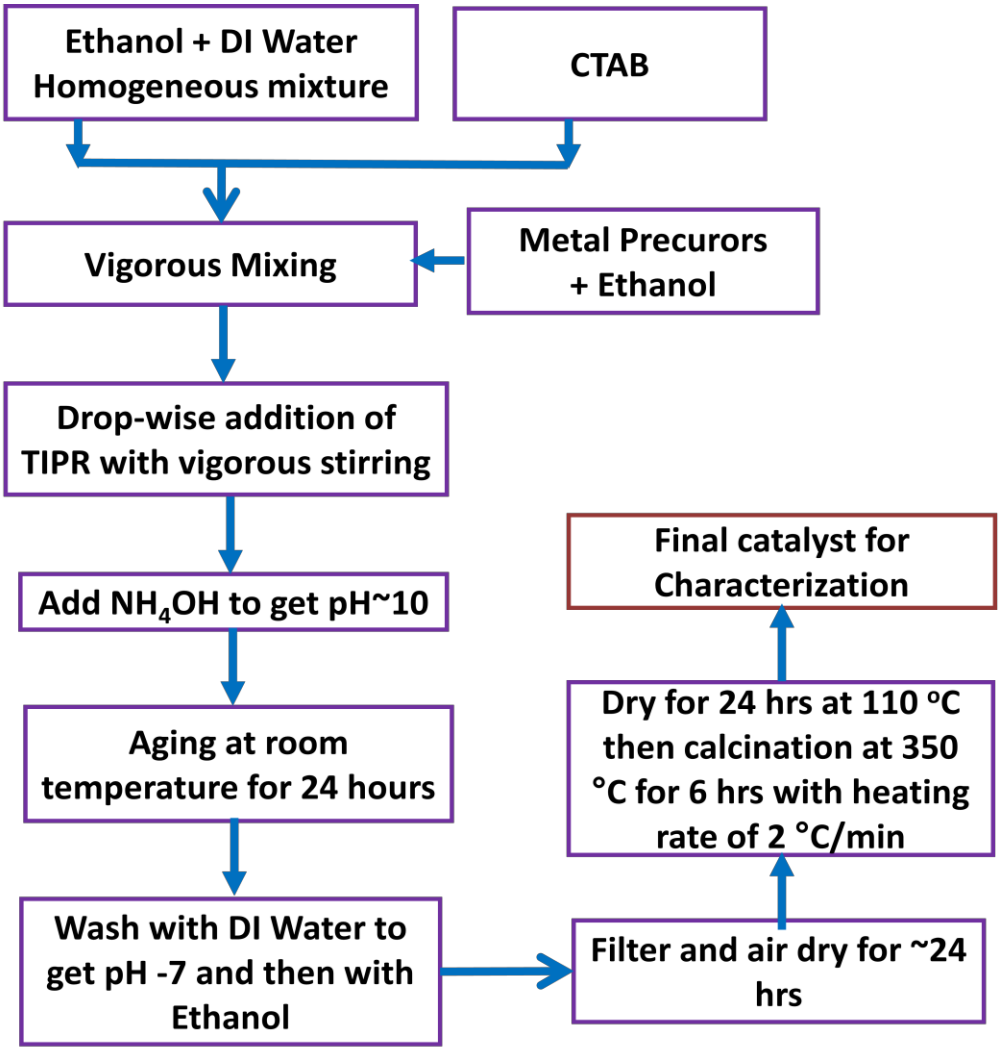

Figure 3.1. Scheme for the synthesis of M-TiO_2 monometallic catalysts

3.3 Catalysts Characterization

3.3.1 Thermo-gravimetric analysis-differential scanning calorimetry (TGA-DSC). Thermo-gravimetric analysis (TGA) and differential scanning calorimetry (DSC) was performed on samples using a SDT Q600 V20.3 Build 14 system (TA Instruments, New Castle, DE, USA). The airflow rate of the environment of the chamber was maintained at 100 mL/min and the sample was heated containing aluminum pan at the rate of 10 °C/min.

3.3.2 N_2 adsorption-desorption isotherm. The specific surface area, pore size, and pore volume of all catalysts were evaluated using a Quantachrome NOVA 2200e instrument. All samples were degassed under vacuum at 150 °C and dosing nitrogen onto the material in a liquid nitrogen bath at 77 K was used to generate the adsorption-desorption isotherms. The surface area of all catalysts were calculated on the basis of the Brunauer-Emmett-Teller (BET) equation from the adsorption branch of the isotherm in a relative pressure (P/P_0) range of 0.07-0.3, where P is absolute pressure and P_0 is saturated vapor pressure. The total pore volume was calculated based on the amount of N_2 adsorbed at a relative pressure close to unity. A dry and clean empty sample cell is weighed and the weight is noted down. About 0.2 g of catalyst is added to the sample cell and placed in a pouch of heating mantle, with a set clamp in place and the cells are inserted and tightened into the fitting. The outgassing process takes ~ 5 h to complete depending on porosity of the sample. After outgassing, the sample cells in the outgassing station are placed in the analysis station. The Dewar flask is filled with liquid nitrogen and placed firmly in the analysis station and the analysis is started.

3.3.3 Inductively coupled plasma optical emission spectroscopy (ICP-OES). The metal content of the catalysts samples was determined using ICP-OES Aglient 710-ES spectrometer. About 75 mg of catalyst sample was dissolved in a mixture of 2 mL of

concentrated hydrofluoric acid (51% HF) and 3 mL concentrated nitric acid (68% HNO_3) followed by heating at about 80 °C for 30 min. The catalyst samples were diluted with de-ionized water before ICP-OES analysis.

3.3.4 X-ray diffraction (XRD) measurements. Powder X-ray powder diffraction (XRD) studies of the samples were carried out using a D8 DISCOVER X-ray diffractometer from Bruker (Bruker Optics, Inc., Billerica, MA) with a position sensitive detector (PSD) from 20°-70° using a step width of 0.014° and scan speed of 1.5 s/step, using Cu Kα radiation generated at 40 mA and 40 kV at the scanning rate of 0.01°/s. The crystal sizes of the CuO and PdO particles were determined using the Scherrer equation (3.1):

$$\tau = \frac{0.9\lambda}{\beta \bullet \cos\theta} \tag{3.1}$$

where τ is the crystal size, λ is the wavelength (λ= 1.5418 mm) of the Cu Kα radiation, β is the full width half maximum of the respective peak and θ is the Braggs angle of diffraction.

3.3.5 H_2-temperature programmed reduction (H_2-TPR*).* The H_2-TPR experiments of the catalysts samples were performed using AutoChem II 2920 Chemical Analyzer from Micro Instrument Corp. (Norcross, GA, USA). In a typical experiment, ~ 0.5 g of the catalyst was placed in a clean quartz sample cell, sandwiched between two wads of quartz wool. The quartz sample cell was fitted with a thermocouple for continuous temperature measurement of the catalyst bed. Before H_2-TPR measurements, the sample was flushed with pure argon (Ar) flow of 50 mL/min at 200 °C for 30 min and then cooled to room temperature. While the temperature was increased to 900 °C at 10 °C/min, a 10% H_2/Ar (50 mL/min) was flown through the catalysts and held at a final temperature for 30 min. The consumption of the hydrogen during the reduction of the catalysts was recorded using a thermal conductivity detector.

3.3.6 Transmission electron microscopy (TEM). The morphology of the catalysts was analyzed using Zeiss Libra 120 transmission electron microscope operated at an accelerating voltage of 120 kV. For analysis, the catalyst sample was dispersed in ethanol and dropped onto a carbon-coated microgrid.

3.3.7 Fourier transform infrared spectroscopy (FTIR). The FTIR spectra were recorded using Shimadzu IR Prestige-21 Fourier transform infrared (FTIR) 8300 spectrometer equipped with mercury-cadmium-telluride (MCT) detector. A potassium bromide (KBr) pellet was used for the sample preparation. The KBr was heated in an oven at 60 °C overnight to eliminate any moisture in the sample. The powdered catalyst (~ 0.01 g) was diluted with a special grade of KBr (~ 0.2 g) in 1:200 ratio and ground into a homogenous powder using a mortar and pestle. The sample was loaded into a 13 mm manual die and pressed to form into a self-supporting pellet. The pellet was mounted on the sample holder and the spectrum was recorded in the range of 4000 to 400 cm^{-1} at 4 cm^{-1} resolutions at an ambient temperature.

3.4 Catalyst Testing for SRM

The operating parameters used in the steam reforming reactions are summarized in Table 3.2. Catalysts were reduced using 4% hydrogen in argon environment at 350 °C temperature for 2 h. The catalytic activity tests were performed under atmospheric pressure in a continuous up flow stainless steel fixed bed reactor (Tube ID: 6.22 mm). The freshly reduced catalyst (~ 1.5 g) was mixed with sand (white quartz, 50-70 mesh, supplier: Sigma-Aldrich) at a ratio of equal volume. The mixture was loaded to the reactor and quartz wool is used at both ends to pack the reactor. Prior to each SRM reaction, the catalyst was activated further *in-situ* at 350 °C for 1 h under 4% H_2 in Ar environment. A feed with a constant methanol/water molar ratio of 1:3 was used in all experiments. The composition of the reaction products and collected condensate were

analyzed using an Agilent 7890B GC equipped with a thermal conductivity detector (TCD) and flame ionization detector (FID). The selectivity to hydrogen was calculated by analyzing the moles of H_2, CO, and CO_2 produced in the SRM reaction. A detailed process flow diagram of the experimental set-up used is shown in Figure 3.2.

Table 3.2

Operating parameters used in steam reforming of methanol

Operation Parameters	Conditions
Temperature (°C)	150-350
Feed Flow Rate (mL/min)	0.1
Gas Hour Space Velocity (hr^{-1} at STP)	2838
Water to Methanol Ratio	3:1
Metal Loading (%)	5-20
Amount of Catalyst (mL)	2
Amount of Sand (mL)	1

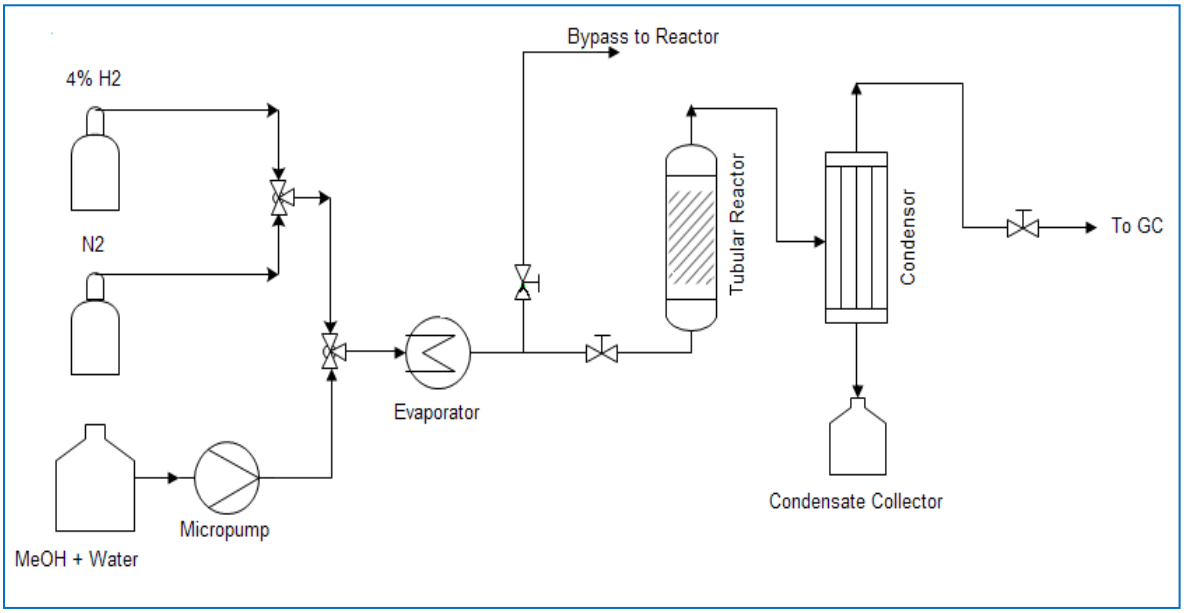

Figure 3.2. Schematic representation of the set-up for steam reforming of methanol to produce hydrogen

The methanol conversion and selectivity towards hydrogen and carbon monoxide were evaluated from equations 3.2-3.4.

$$X_{Methanol} = \frac{CH_3OH\ moles\ converted}{CH_3OH\ moles\ fed} X\ 100\% \tag{3.2}$$

$$S_{H_2} = \frac{H_2\ molesin\ product}{H_2\ molesin\ product + 2\ X\ CH_4\ molesin\ product} X\ 100\% \tag{3.3}$$

$$S_{CO} = \frac{COmolesin\ product}{CO_2\ molesin\ product + COmolesin\ product + CH_4\ molesin\ product} X\ 100\% \tag{3.4}$$

CHAPTER 4

Results and Discussion

4.1 Catalysts Characterization

4.1.1 TGA-DSC. Figure 4.1 shows the typical TGA-DSC profile of mesoporous-TiO_2 recorded in air.

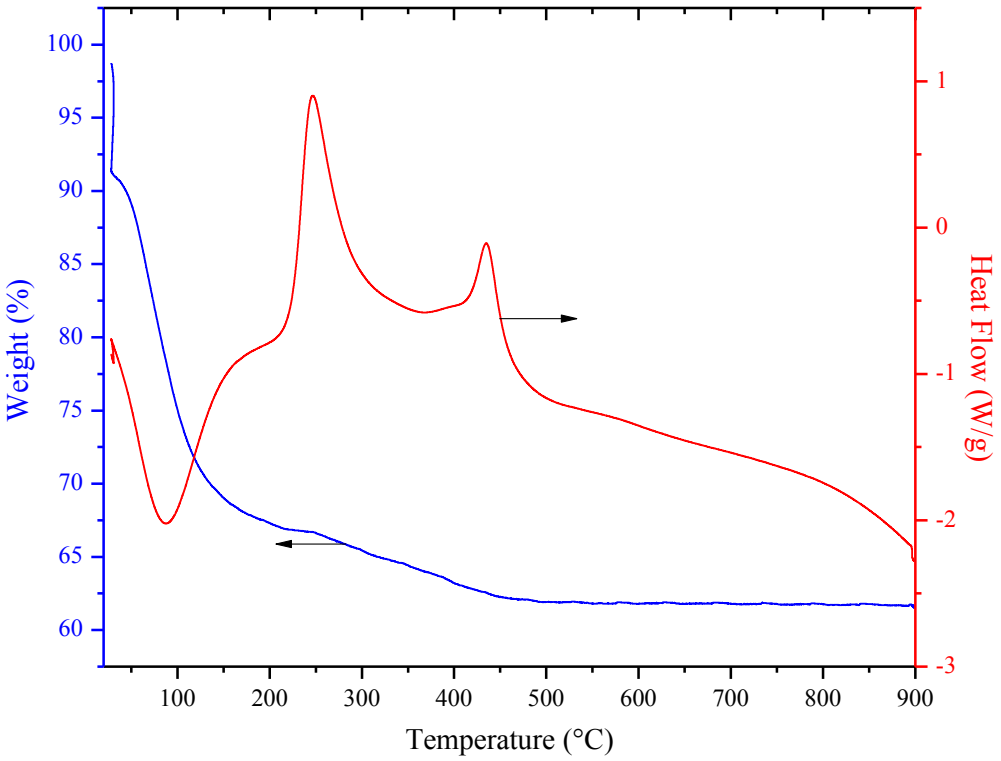

Figure 4.1. TGA-DSC profile of mesoporous-TiO_2

The profile or thermogram shows weight loss at two stages. The first one is located below 180 °C and is associated with a strong endothermic peak centered at ~ 85 °C. This weight loss is attributed to removal of adsorbed water on the surface of mesoporous-TiO_2. The second weight loss can be attributed to the removal of CTAB used as the templating agent for mesoporous structure, which also corresponds to an exothermic peak between 220 - 300 °C in the DSC scan. A second exothermic peak is observed at ~ 450 °C, but with insignificant weight loss of the

material. Hence, this peak can be attributed to the transition from amorphous to the crystalline phase of TiO_2.

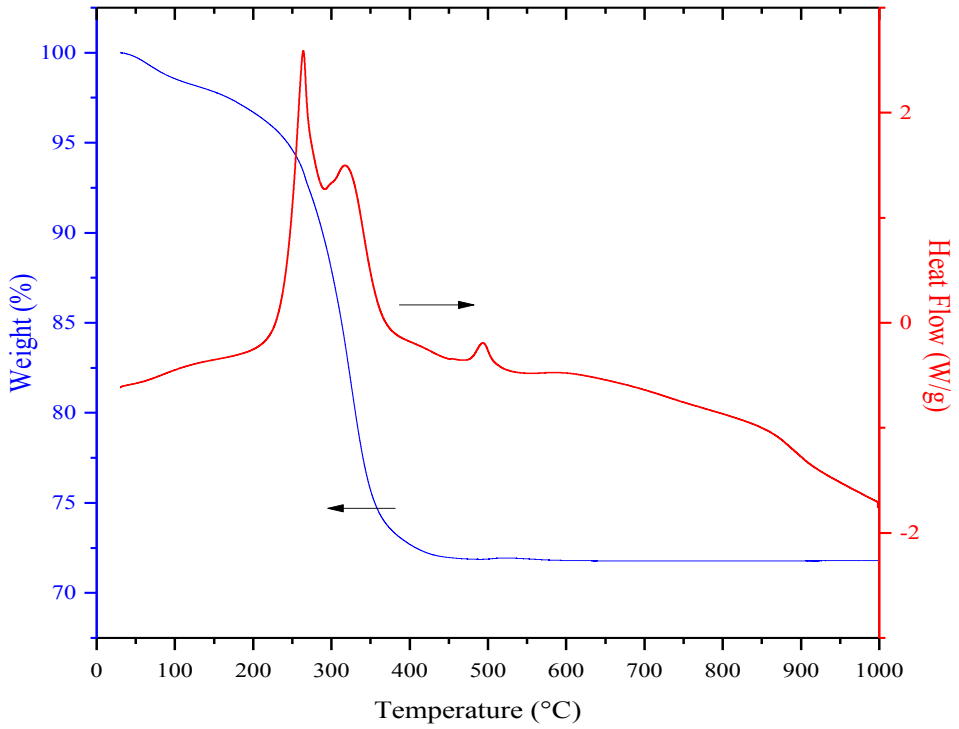

Figure 4.2. TGA-DSC profile of 10%Co-TiO_2 obtained by one-pot synthesis

Figure 4.2 shows the typical TGA-DSC profile of 10%Co-TiO_2 recorded in air. There are two significant weight loss stages in the TGA profile. The first one is between 20-100 °C, which can be attributed to the removal of adsorbed water on the surface of mesoporous-TiO_2. The second weight loss in the range of ~ 200-400 °C can correspond to the removal of CTAB. This coincides with an exothermic peak ~ 250 °C due to the removal of CTAB. The second exothermic peak at ~ 300 °C could correspond to the decomposition or condensation of the hydroxyl groups as reported by Arsalanfar et al. [48]. A third exothermic peak is observed at 450 °C with insignificant weight loss of the material. Hence, this peak may be attributed to the transition from amorphous to the crystalline phase of TiO_2. Darzi et al. reported at peak at 470

°C in the DSC curve attributing to the crystallization of amorphous phase to anatase of mesoporous-TiO_2 [49].

Figure 4.3 shows the TGA-DSC profiles of different Zn-TiO_2 samples with Zn loading varied from 5-20%.

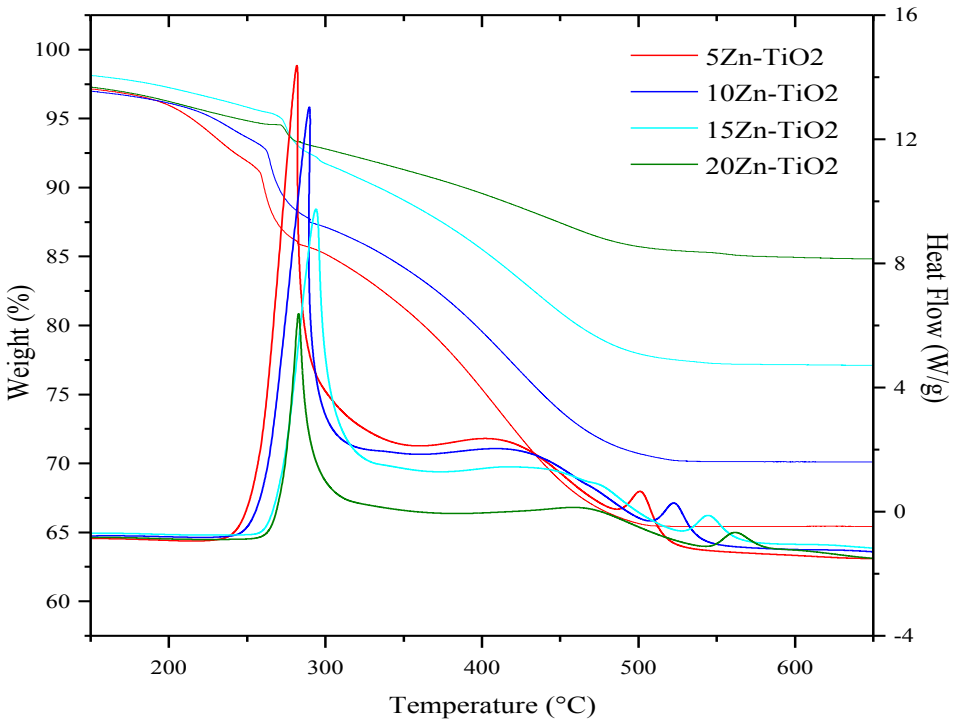

Figure 4.3. TGA-DSC profiles of 5-20%Zn-TiO_2 recorded in an atmosphere of air

All profiles show one significant weight loss at ~ 250-450 °C, which can be attributed to removal of the template, CTAB. The first exothermic peak in DSC observed at ~ 275 °C for all catalyst corresponds to the removal of the template, also observed by Lee et al. [50]. They observed a peak ~ 290 °C corresponding to the removal of CTAB in DSC curves of mesoporous titania via sol-gel method. A second exothermic peak is observed between ~500-560 °C for all catalyst with insignificant weight loss of the material. These peaks can be attributed to the crystallization of amorphous to the crystalline phase of TiO_2 [49]. It can also be observed that

with the increase in Zn loading from 5 to 20 %, the crystallization temperature increased from ~500 to 560 °C. There is no exothermic peak for decomposition of hydroxyl group, as observed in the 10%Co-TiO_2 sample. The crystallization temperature was observed to increase from ~450 °C to ~ 500 °C with the addition of metal on mesoporous titania with Co and Zn samples showing a delay in crystallization.

4.1.2 Textural properties. The N_2 adsorption-desorption isotherms for mesoporous-TiO_2 and different metal incorporated mesoporous-TiO_2 with metal loading of 10 wt% are depicted in Figure 4.4. Based on IUPAC classification, all isotherms for monometallic catalysts resemble the Type IV isotherm, a typical characteristic for mesoporous materials [51].

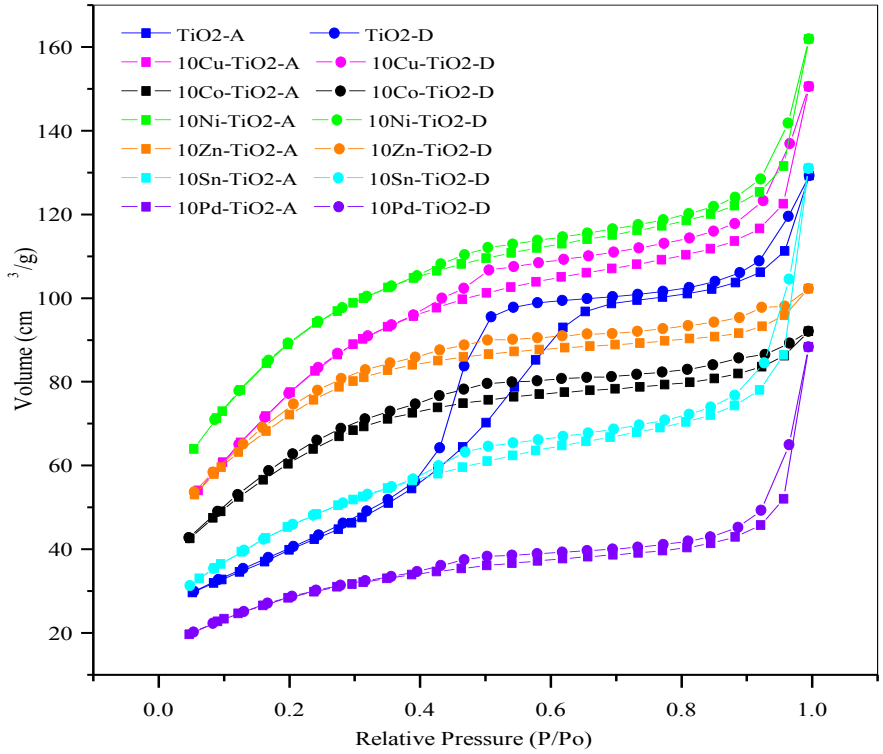

Figure 4.4. N_2 adsorption-desorption isotherms for mesoporous-TiO_2 and M-TiO_2 catalysts

From the isotherms, a linear increase of nitrogen uptake at a low relative pressure (P/P_0= 0-0.23) can be observed from the monolayer-multilayer adsorption on the pore walls. At higher relative

pressure (P/P_0=0.43-0.97), multilayer adsorption occurs, and it is associated with hysteresis loop indicative of capillary condensation. Lastly, a sharp rise in N_2 uptake at relative pressure above 0.97 is observed due to the presence of interparticle pores. Mesoporous-TiO_2 consists of a H2 type hysteresis loop that corresponds to the inkbottle shaped pores. However, the Figure 4.4 also shows that the shape of the hysteresis loop changes from H2 to H4 upon addition of metal particles indicating a significant change in the textural properties. The H4 hysteresis loops are generally associated with the slit-like pores, which are usually eclipse shaped [52].

The BET surface areas, pore sizes, and pore volumes of the mesoporous-TiO_2 and different M-TiO_2 catalysts obtained from N_2 adsorption-desorption studies are presented in Table 4.1. The surface area, pore diameter, and pore volume of catalysts ranged from 99.86-309.79 m^2/g, 2.53-4.93 nm, and 0.08-2.03 cm^3/g, respectively, depending on the type of metal incorporated into mesoporous-TiO_2. Mesoporous-TiO_2 support has a specific surface area of 146.56 m^2/g; however, addition of metal particles led to the significant increase in surface area except for Pd-TiO_2. Thus, it is evident that the addition of metals into titania causes structural changes in the mesoporous-TiO_2 support.

Our results with addition of metals to TiO_2 are similar to the increase in surface area upon addition of metal ions to ZrO_2. Youn et al. [53] reported that the addition of small amount of metal cations into zirconia support led to increase in surface area due to enhancement of the structural stability of the cubic or tetragonal phase. The high surface area of the catalysts in the present study is mainly due to the highly mesoporous nature of the TiO_2 support as evident in the N_2 adsorption-desorption isotherm with hysteresis loops [54]. The crystallization of mesoporous-TiO_2 upon calcination leads to the collapse of the mesoporous structure due to the increased crystallite size, thus decreasing the surface area. The degree of decreased surface area

depends upon the degree of crystallization. Clearly, the metal loading in the titania support enhance the structural stability of the anatase crystalline phase. However, this was not observed in the case of 10%Pd-TiO_2, where the specific surface area diminishes after addition of Pd metal causing a decrease in total pore volume and pore size when compared to mesoporous-TiO_2. The decrease in surface area of 10%Pd-TiO_2 can be attributed to the large sizes of Pd metal particles. This will be discussed in more detail during the discussion of XRD results.

The actual metal loading in mesoporous-TiO_2 also plays a significant role in the actvities of the catalyst. The results from our analysis, determined using ICP-OES, are also shown in Table 4.1.

Table 4.1

Surface areas, pore sizes, pore volumes, and actual metal loadings of different M-TiO_2 catalysts

Catalyst	Surface Area (m^2/g)	Pore Size (nm)	Pore Volume (cm^3/g)	Actual Metal Loading (wt %) ICP-OES
TiO_2	146.56	4.70	0.17	0
10Cu-TiO_2	285.57	2.65	0.19	10.6
10Ni-TiO_2	309.79	2.63	0.20	13.9
10Co-TiO_2	215.14	2.65	0.14	13.3
10Sn-TiO_2	164.29	4.93	0.13	5.26
10Pd-TiO_2	99.68	3.23	0.08	5.32
10Zn-TiO_2	250.24	2.53	0.16	12.52

The metal loadings of different 10 wt% monometallic catalysts varied in the range of 10.6 to 13.9 %, except for samples of 10%Sn-TiO_2 and 10%Pd-TiO_2. For Sn and Pd based catalysts, the

loading was found to be considerably lower (5.26 and 5.32 %) than the intended loading of 10%. While, the higher loading of metal can be attributed to the more loss of titania particles or precursor, the lower metal loading in some cases could be due to the loss of metal particles or metal precursors during the catalysts preparation.

Table 4.2 presents the surface areas, pore sizes, pore volume, and actual metal loadings of 5-20 %Zn-TiO_2 catalyst obtained by N_2 adsorption-desorption studies. An interesting behavior was observed in surface area variation when the Zn loading was increased from 0 to 20 wt%. As the loading was increased from 0 to 15 %, the surface area increased from ~146 to ~257.5 m^2/g. However, with further increase in Zn loading to 20%, a drastic reduction in surface area to 140.11 m^2/g was observed.

Table 4.2

Surface areas, pore sizes, pore volumes, and actual metal loading of different Zn-TiO_2 catalysts

Catalyst	Surface Area (m^2/g)	Pore Size (nm)	Pore Volume (cm^3/g)	Actual Metal Loading (wt %) ICP-OES
5Zn-TiO_2	178.77	2.9557	0.1321	5.2
10Zn-TiO_2	250.24	2.5274	0.1581	12.52
15Zn-TiO_2	257.50	2.7227	0.1753	12.14
20Zn-TiO_2	140.11	3.2291	0.1131	17.18

The first trend in surface area variation can be explained as discussed before based on the delay in crystallization due to the presence of Zn atoms. This delay in crystallization of TiO_2 was observed to increase with the increase in Zn loading, as presented before in our TGA-DSC results. Thus, up to 15% loading, Zn atoms hinder the crystallization of TiO_2, which avoids the collapse of the mesoporous structure. However, the decreased surface area of catalysts at higher

Zn loading (i.e. above 15%), caused Zn atoms not only act as impurity hindering the crystallization, but they also interfere in the formation of mesoporous structure. The observed lower surface area of 20%Zn-TiO_2 compared to mesoporous-TiO_2 is attributed to this relatively less porous nature of the material.

4.1.3 X-ray diffraction. X-ray Diffraction is an important technique used to investigate the ordered mesoporous materials and also to characterize the materials' crystallization behavior. Figure 4.5 represents the x-ray diffraction pattern of mesoporous-TiO_2 and different M-TiO_2 samples.

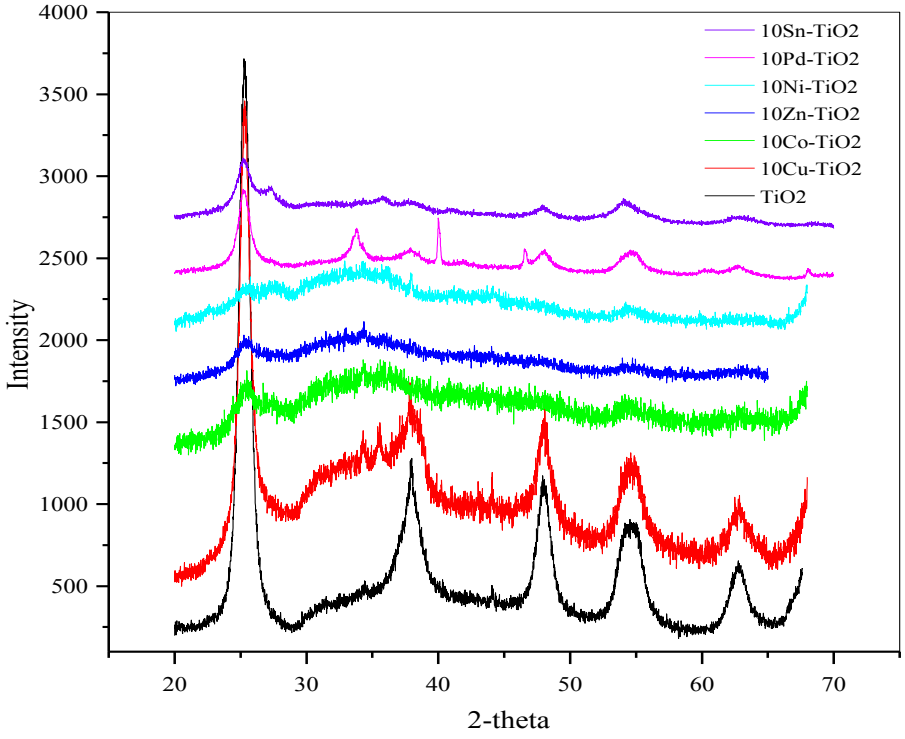

Figure 4.5. XRD patterns of different M-TiO_2 catalysts with 10 wt% metal loading

TiO_2 has three phase transitions, which includes rutile (tetragonal), anatase (tetragonal), and brookite (orthorhombic). For mesoporous TiO_2, strong diffraction peaks at about 25°, 38°, 48°, 55°, 62° are observed, which are characteristics of the pure anatase-type TiO_2 and reveal the

absence of both the rutile and brookite phase [27]. These peaks are indexed as (101), (004), (200), (105), and (211) planes, respectively [55]. Addition of metal led to a decrease in intensity of these peaks, indicating a lower degree of crystallization. However, this decrease in crystallization appears to be strongly dependent on the type of the metal. For example, while Cu showed an insignificant change in intensity, the presence of Ni did not show any clear peak in XRD. For 10%Co-TiO_2, 10%Zn-TiO_2, 10%Ni-TiO_2, and 10%Sn-TiO_2 samples no peaks attributed to the metal or metal oxides in the XRD spectra were observed. This could be due to the non-crystalline phase, highly uniform dispersion, and very small sizes, which are x-ray amorphous and not detected by XRD technique [56]. The XRD spectrum of 10%Cu-TiO_2 exhibits two peaks at 2-theta 35.5° and 38.7°, ascribed to the monoclinic CuO crystal phase, assigned to (002) and (111) planes, respectively [57]. The XRD spectra of 10%Pd-TiO_2 also showed a peak at 2-theta values of 42.1° assigned to (111) crystalline plane of PdO [58].

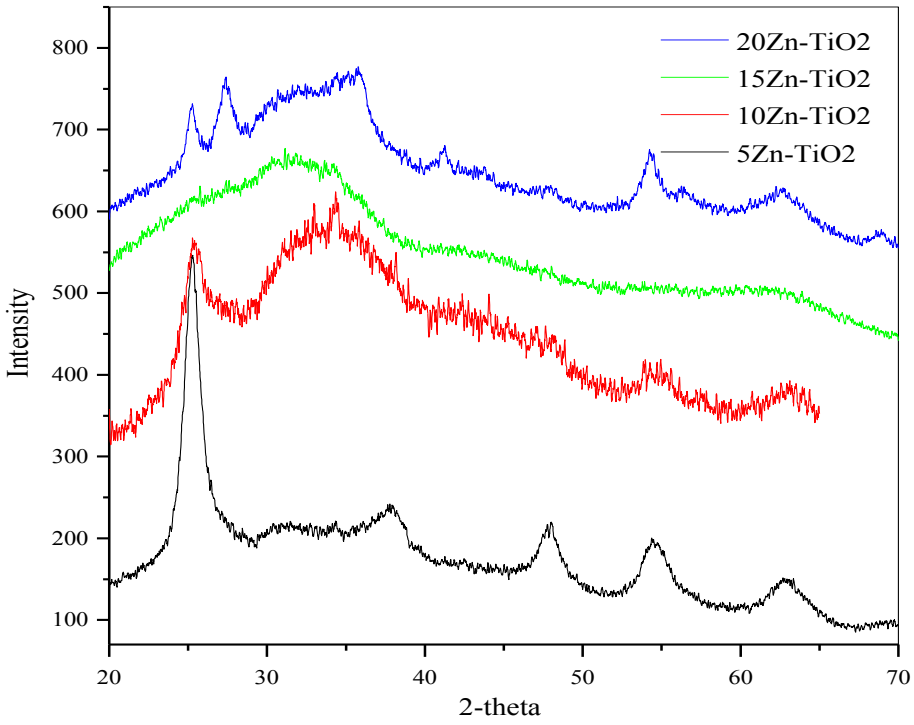

Figure 4.6. XRD patterns of 5-20% Zn-TiO_2 catalysts

Figure 4.6 shows the x-ray diffraction pattern of 5-20%Zn-TiO_2 samples. XRD studies show that the addition of metal particles to TiO_2 matrix result in decreased peak intensities. It indicates that the presence of metal atoms hinder or delays the TiO_2 crystallization process, which was also confirmed by the TGA-DSC studies. The rate of crystallization during heat treatment depends on the rate of atomic diffusivity of titanium ions. However, the presence of metal atoms could be acting as an impurity or adatoms decreasing the mobility of Ti ions resulting in decreased diffusivity and subsequently decreased crystallization property [59]. Thus, the higher surface area of M-TiO_2 compared to TiO_2 can be attributed to relatively lower extent of crystallization upon metal addition.

The particle sizes of catalyst and crystal sizes of the CuO and PdO calculated using Scherrer equation (3.1) are shown in Table 4.3**.** The TiO_2 crystal size decreases upon metal loading, confirming low crystallinity by XRD. The metal crystal size of Pd is ~ 49.39 nm, which is large and explains the decrease in specific surface area.

Table 4.3

Particle sizes of TiO_2 and metal crystals

Catalyst	TiO_2 Crystal Size (nm)	Metal Crystal Size (nm)
TiO_2	17.18	-
10%Sn-TiO_2	7.52	-
10%Cu-TiO_2	9.84	20.94
10%Co-TiO_2	4.03	-
10%Pd-TiO_2	8.78	49.39
10%Zn-TiO_2	6.79	-
5%Zn-TiO_2	7.29	-

4.1.4 TPR. Temperature programmed reduction (TPR) is a technique that gives information about the reduction behavior and reduction temperature of metal oxides interacting with the support. Mesoporous-TiO_2 is known to have a strong metal-support interactions effect (SMSI) that can affect the properties of the catalyst [60]. Therefore, TPR study of M-TiO_2 catalysts will provide information on the interaction between the metal species and titania support, which can be correlated to its SRM activity. Figure 4.7 depicts the TPR of mesoporous-TiO_2 and different M-TiO_2 catalysts. TPR was conducted on TiO_2 support at the same TPR conditions used for the catalyst samples to detect any hydrogen consumption by the support. The TiO_2 support showed a broad low intensity reduction peak at about 530 °C and another small peak initiated at about 900 °C, indicating that some of the TiO_2 was also reduced [61]. Hwang et al. [62] also reported a broad band centered at 560°C corresponding to surface reduction of TiO_2. The TPR profile of 10%Pd-TiO_2 shows a sharp reduction peak centered at 91 °C, which is due to the reduction of PdO to metallic Pd (Pd^{2+} to Pd). A similar behavior was observed with Pd supported on TiO_2 by Pérez-Hernández et al. [4]. It has been reported that a peak in the range of 90-160 °C is associated with PdO particles [63, 64]. A negative peak is also observed around 250 °C that could be attributed to the release of H_2 from decomposition of the palladium hydride formed previously with H_2 [4, 65]. For 10%Cu-TiO_2, there are two peaks that can be ascribed to two step reduction of species that are more or less interacting with the support [66]. The first peak ~ 150 °C could be due to the reduction of CuO to Cu_2O species that is highly dispersed and interacting with TiO_2 support as confirmed by XRD studies. The second peak ~ 170 °C is mainly due to reduction of Cu_2O to Cu. Smith et al. [67] also reported this two-step reduction process of $CuO \rightarrow Cu_2O \rightarrow Cu^0$ in Cu/SiO_2 catalyst. The TPR of 10%Co-TiO_2 showed a shoulder in the range of 350-600 °C before the broad reduction peak, which could be attributed to the reduction

of Co_3O_4 to CoO. The broad reduction peak at ~600-890 °C could be assigned to the reduction of CoO to metallic Co. There are no H_2 consumption peaks that can be due to the reduction of the titania support. Bayram et al. [68] reported a doublet in the TPR profile of Co/CeO_2 and found that the first peak was attributed to the reduction of Co_3O_4 to CoO and the second peak to reduction of CoO to metallic Co. The area under the curve was used to calculate the ratio of the second peak to the first peak, to help assign the peaks with the appropriate reduction steps. The observed ratio of 1: 3 was in agreement with the stoichiometry of the stepwise reduction of Co_3O_4 to CoO to metallic Co.

In contrast to the TPR profile of $Co\text{-}TiO_2$, $10\%Ni\text{-}TiO_2$ shows different features. The main sharp peak at 400 °C that can be attributed to large NiO particles with no interaction with the titania support [69]. The observed small peak in the range of 450-600 °C can be attributed to NiO strongly reacting with the TiO_2 support. Vita et al. [70] reported he studies of NiO supported on CeO_2 where two reduction peaks were observed at 400 °C and 500 °C. They attributed these peaks to NiO reacting with the CeO_2 support weakly and strongly, respectively. It was suggested that NiO reduction occurs to a great extent during the first step due to catalysts with low nickel content. The second peak of NiO interacting strongly with the support is related to the catalytic activity in the SRM.

In the TPR profile of $10\%Zn\text{-}TiO_2$, three reduction peaks are observed due to H_2 consumption at ~ 430 °C, 650 °C, and 750 °C. According to literature, these peaks can be attributed to the reduction of the spinel-like $ZnTi_2O_4$ species. Hull et al. [71] reported spinel-like species for $ZnFe_2O_4$ at three reduction temperatures due to the reduction of the spinel to Fe_3O_4, then Fe_3O_4 to FeO, and lastly FeO to Fe for the steam reforming of ethanol (SRE). The advantages of spinel-like species are low acidity, thermal stability, and resistance to coking, and

thus make them favorable for steam reforming reactions. In conclusion, mixed metal oxides that contain spinel-like structures with zinc were linked to the catalytic active sites in steam reforming processes. It also can be observed that reduction is not complete even after 1000 °C due to reduction of the TiO_2 support.

Lastly, the TPR profile for 10%Sn-TiO_2 shows three distinct reduction peaks contributed to an occurrence of a more complex reduction. The first reduction peak around 300 °C could be attributed to the reduction of Sn^{4+} to Sn^{2+} and the second reduction peak around 500 °C could represent the reduction of Sn^{2+} to metallic Sn. Our results are similar to that observed by Li et al. [72]. The last reduction peak ~ 700 °C could be attributed to the reduction of the support [73].

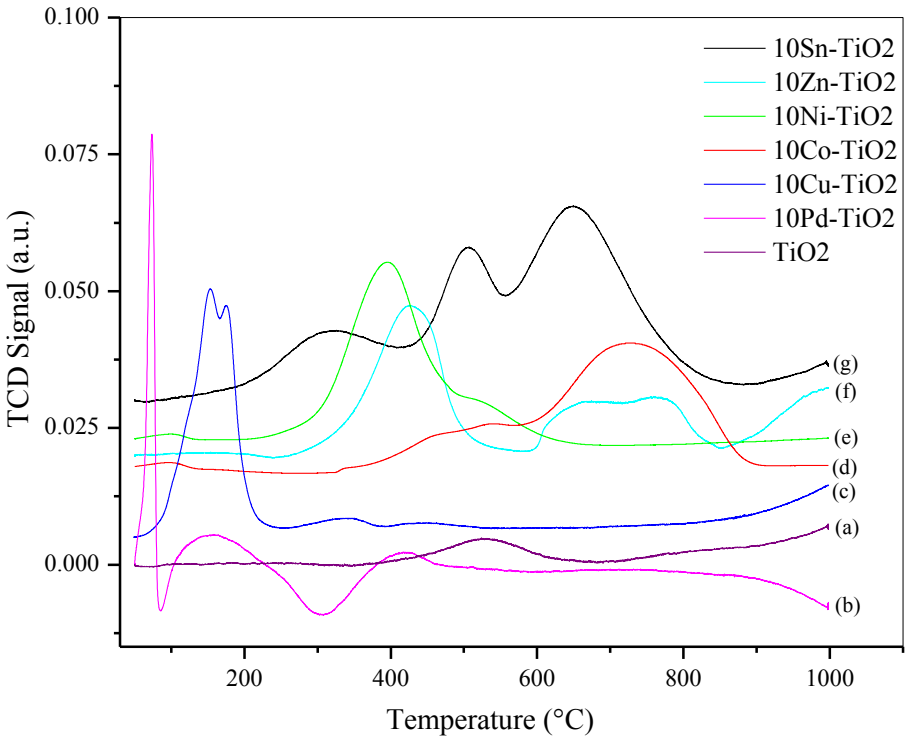

Figure 4.7. TPR profiles of different M-TiO_2 catalysts with 10 wt % metal loading

4.1.5 TEM. Metal containing TiO_2 and mesoporous-TiO_2 catalyst were studied by transmission electron microscopy (TEM). The TEM images of (a) mesoporous-TiO_2, (b) 10%Co-TiO_2, (c) 10%Sn-TiO_2, and (d) 10%Zn-TiO_2 are shown in Figure 4.8. Figure 4.8(a), (c),

and (d) displays the high mesoporous structure even after the addition of metal in each case. Figure 4.8(b) indicates the uniform distribution of Co metal supported on mesoporous-TiO_2.

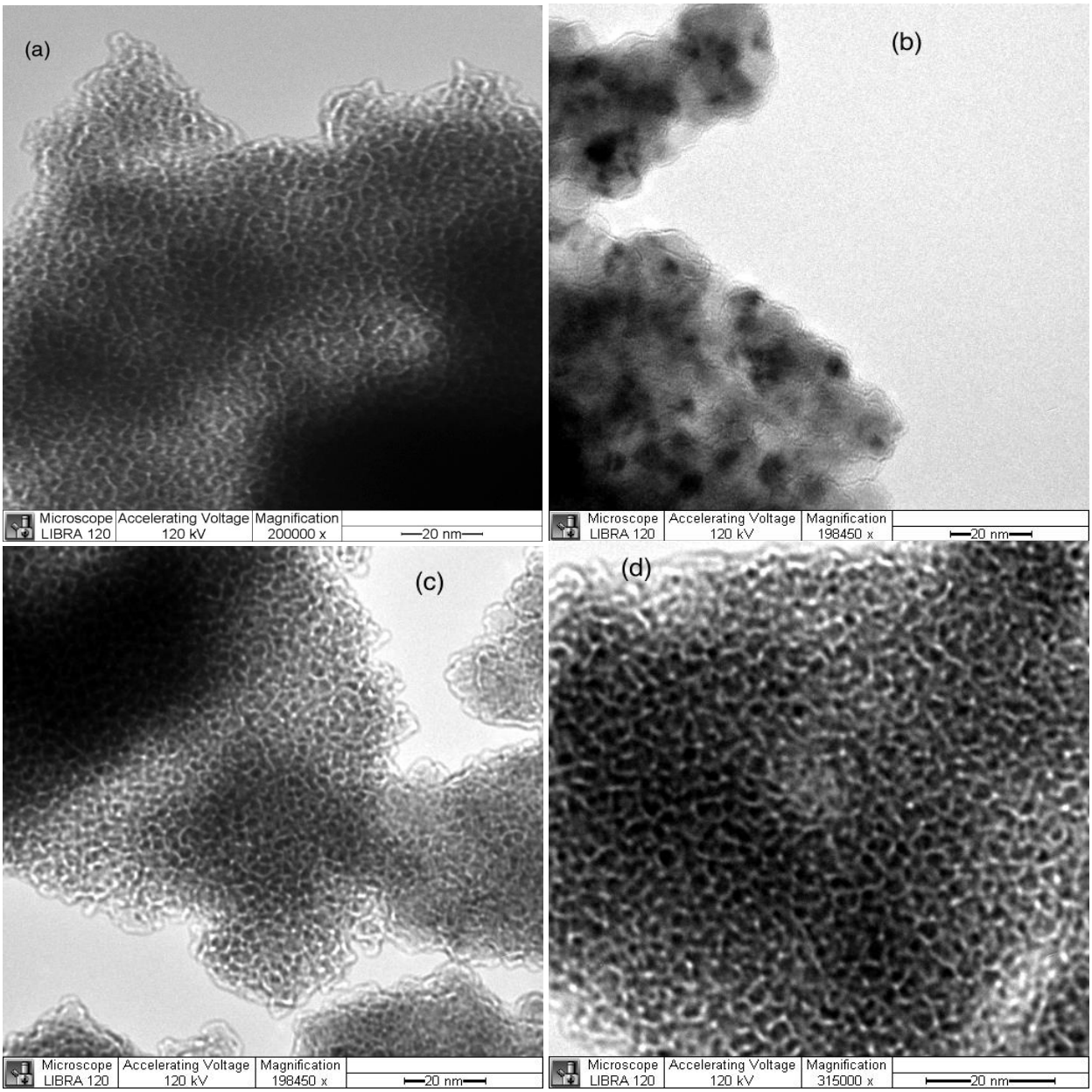

Figure 4.8. TEM images of (a) mesoporous-TiO_2 (b) 10%Co-TiO_2 (c) 10%Sn-TiO_2 (d) 10%Zn-TiO_2 catalysts

4.1.6 FTIR. The FTIR studies were done to understand further the interaction between the different metals and the support. The spectra of as-prepared and calcined samples of

mesoporous-TiO_2 and different M-TiO_2 catalyst are shown in Figure 4.9 (a-g). All as-prepared samples contain a doublet band centered at ~ 2925 cm^{-1} and 2854 cm^{-1}, with a distinct band around ~ 1500 cm^{-1} contributed to the symmetric C-H and asymmetric CH_2 vibrations of the organic template, CTAB, that disappears in the calcined samples confirming its complete removal. These results are in good agreement with previous studies [55]. Only the 10%Zn-TiO_2 sample had peaks in the calcined samples from the organic template, which was not completely removed after calcination due incomplete removal of surfactant. The strong band in the range of 900 - 400 cm^{-1} is associated with vibration modes of TiO_2 (Ti-O-Ti). The broad adsorption bands in the range of 3800 – 3000 cm^{-1} in all samples are assigned to the presence of –OH stretching and the intensity of the peaks decreases and shifts to the left due to condensation of the –OH groups. The presence of the adsorption band in all samples around ~ 1630 cm^{-1} could be assigned to the O-H bending vibration that can also arise from water absorbed on the surface from the atmosphere [74]. The adsorption bands ~ 2350 cm^{-1} corresponds atmospheric CO_2, also observed by Khalid et al. [75].

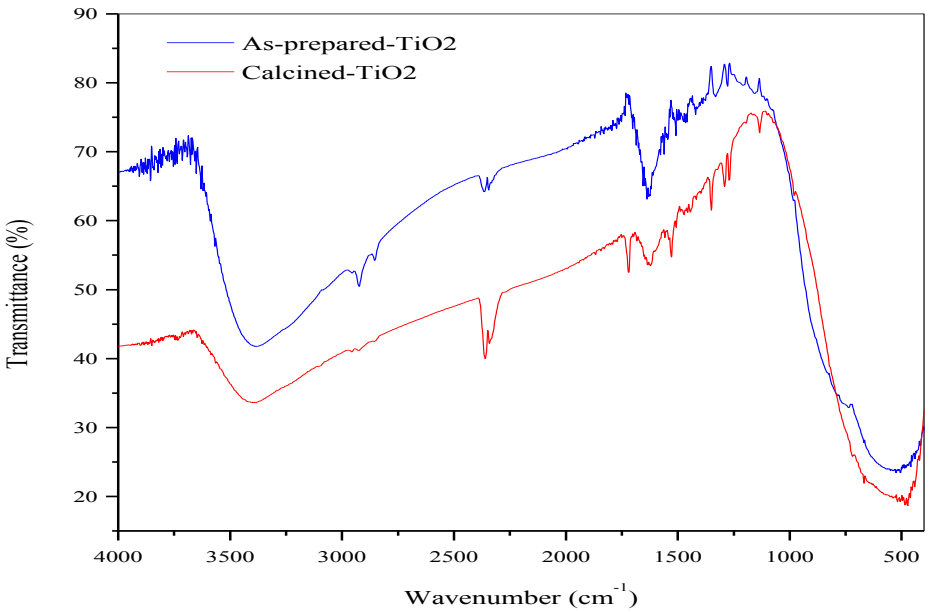

(a)

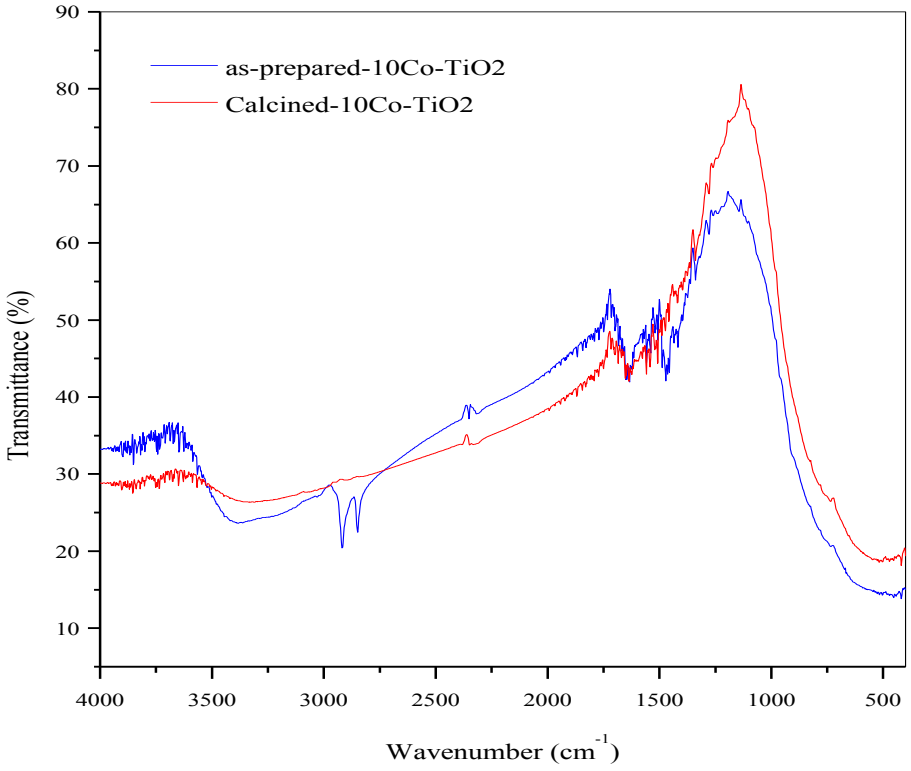
as-prepared-10Co-TiO2
Calcined-10Co-TiO2
Transmittance (%)
Wavenumber (cm-1)
90
80
70
60
50
40
30
20
10
4000
3500
3000
2500
2000
1500
1000
500

(b)

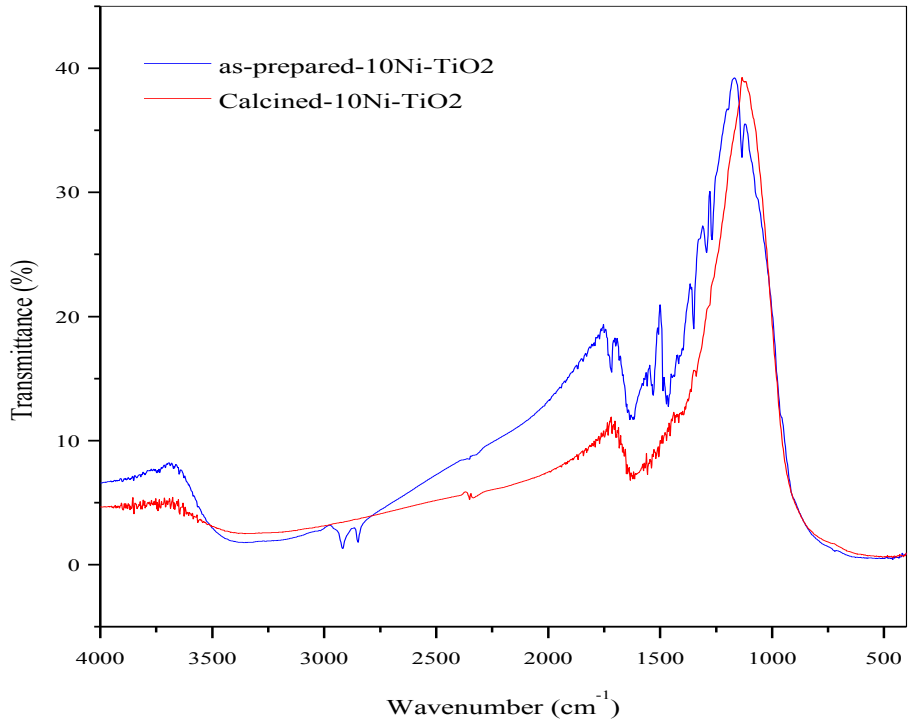
as-prepared-10Ni-TiO2
Calcined-10Ni-TiO2
Transmittance (%)
Wavenumber (cm-1)
40
30
20
10
0
4000
3500
3000
2500
2000
1500
1000
500

(c)

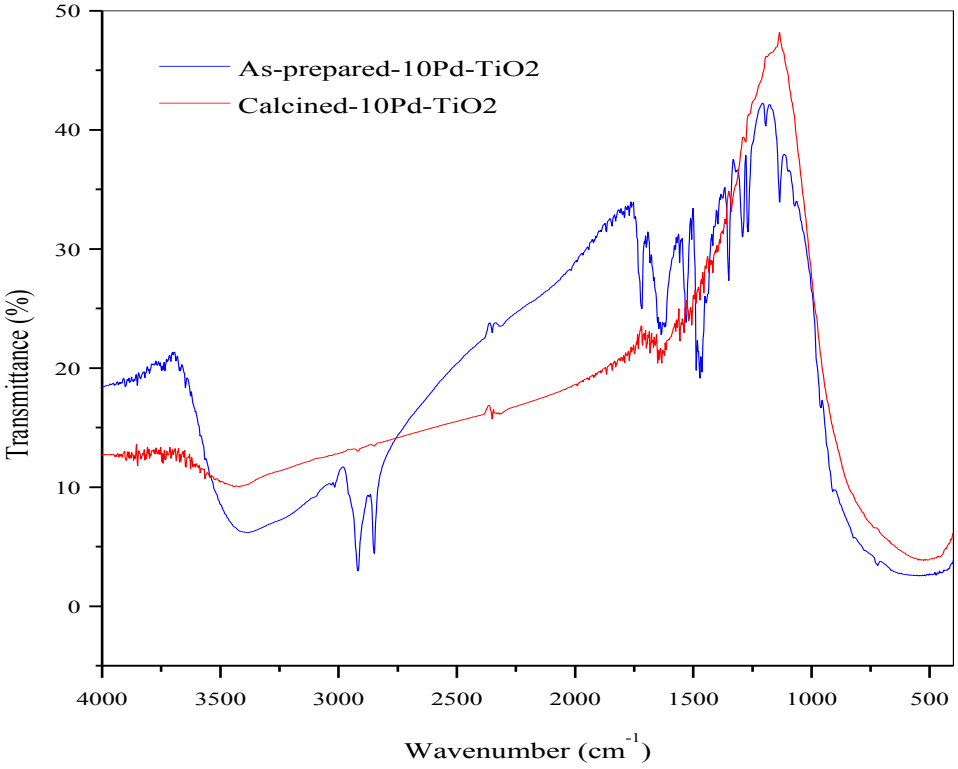
As-prepared-10Pd-TiO2
Calcined-10Pd-TiO2
Transmittance (%)
Wavenumber (cm-1)
50
40
30
20
10
0
4000
3500
3000
2500
2000
1500
1000
500

(d)

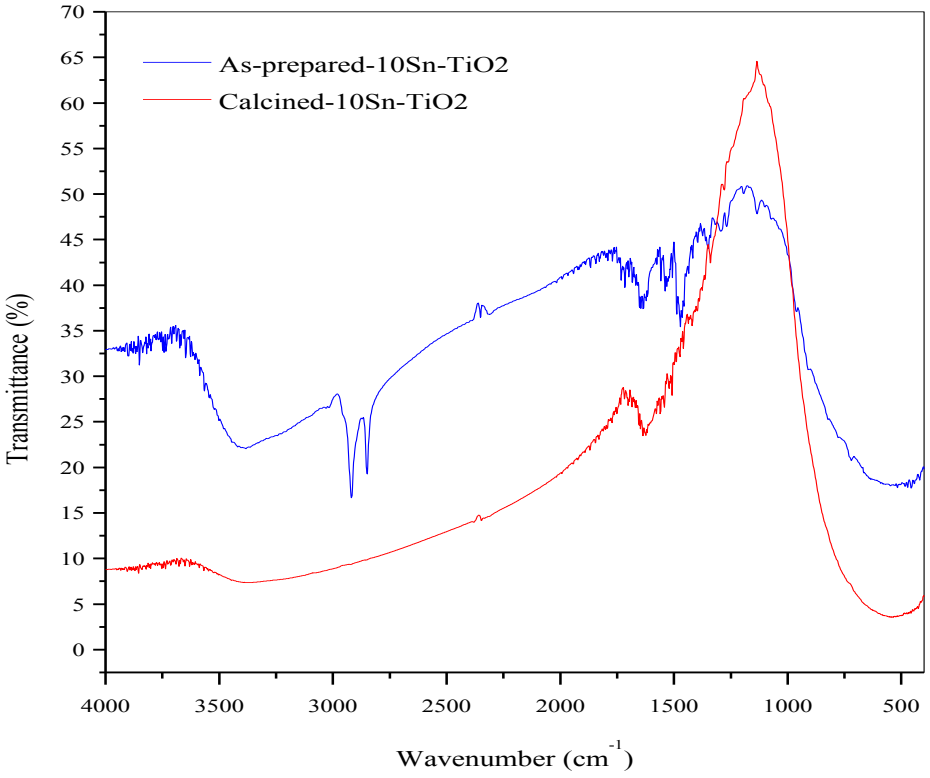
As-prepared-10Sn-TiO2
Calcined-10Sn-TiO2
Transmittance (%)
Wavenumber (cm-1)
70
65
60
55
50
45
40
35
30
25
20
15
10
5
0
4000
3500
3000
2500
2000
1500
1000
500

(e)

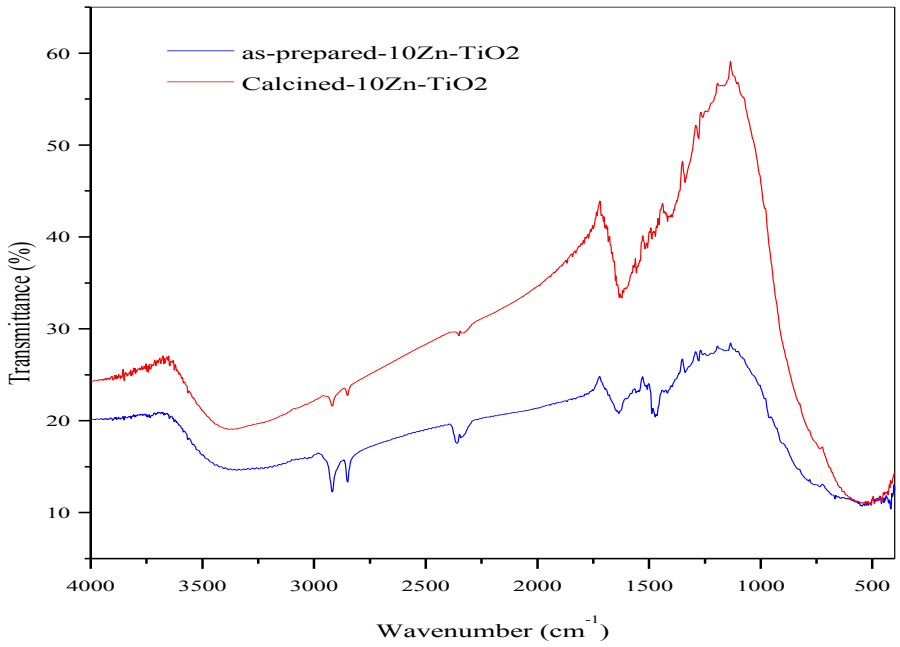

(f)

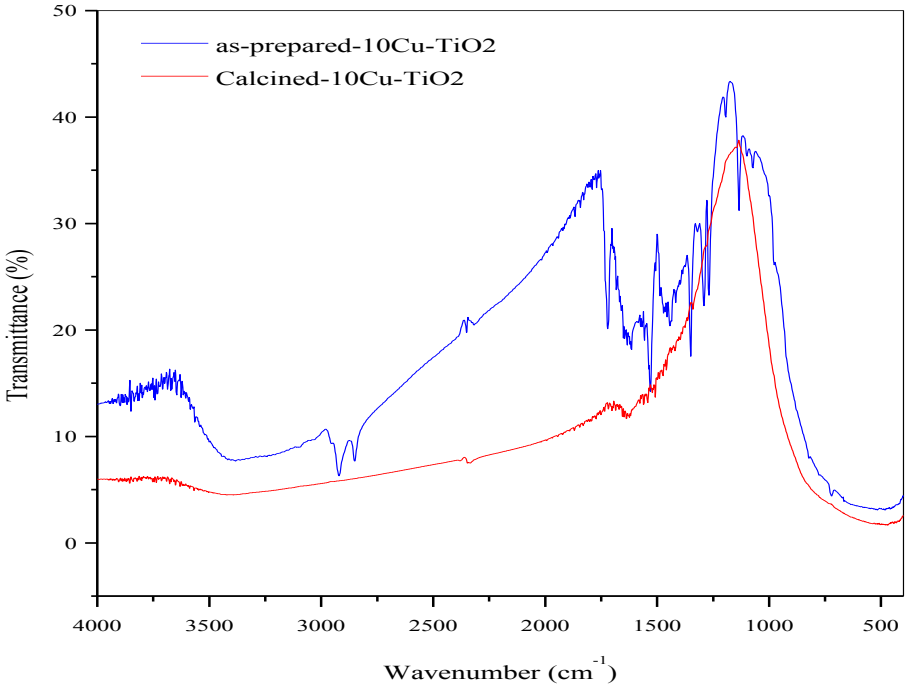

(g)

Figure 4.9. FTIR spectra of as-prepared and calcined samples of (a) mesoporous-TiO_2 (b) 10%Co-TiO_2 (c) 10%Ni-TiO_2 (d) 10%Pd-TiO_2 (e) 10%Sn-TiO_2 (f) 10%Zn-TiO_2 (g) 10%Cu-TiO_2 catalysts

4.2 Catalysts Testing for SRM

Table 4.4 summarizes the effect of temperature on the steam reforming of methanol activity and selectivity of different M-TiO_2 catalysts. Methanol conversion was higher at higher reaction temperature for all M-TiO_2 catalysts. This is consistent with the work of Pèrez-Hernández et al. [13], who observed higher conversion at the maximum reaction temperature of 375 °C with Ni/CeO_2-ZrO_2 catalyst. More significantly, our studies show that the catalyst can have a significant influence on the methanol conversion depending on the metal used. The catalytic activity of 10%Co-TiO_2 increased to 71.83% with the increase in temperature to 350 °C. The selectivity of CO and CH_4 decreases with the increase in temperature, while the selectivity of H_2 and CO_2 increases showing promotion of the WGS reaction in equation (2.3). The low activity of 10%Co-TiO_2 could be due to the higher reduction temperature of the Co metal species. The catalytic activity of 10%Ni-TiO_2 increased to 86.22% with the increase in temperature to 350 °C and showed high selectivity for H_2 and CO suggesting that the main reaction was methanol decomposition as shown in equation (2.1). Further, this reaction showed SRM activity for temperature as low as 150 °C. The activity of 10%Ni-TiO_2 does not favor the WGS reaction and promotes high levels of CO, but the catalyst is highly active due to the NiO particles strongly reacting with the support. Pèrez-Hernández et al. [13] also reported the same trend over Ni-based catalysts supported on CeO_2-ZrO_2 mixed oxides. For 10%Cu-TiO_2, the catalytic activity is low and increases with the increase in temperature, but only up to 28.22% at 350 °C. The selectivity towards H_2 and CO increases with the increase in temperature, confirming the WGS reaction is not favorable with 10%Cu-TiO_2 catalyst and as stated previously, the active site could be covered with Cu crystallites causing low performance. The 10%Pd-TiO_2 catalysts also showed activity at 150 °C, but with only 8.04% conversion. The

activity of the catalyst increased to 97.84% with an increase in temperature to 350 °C. The selectivity towards hydrogen decreased as the selectivity to CH_4 increased. However, the selectivity toward CO decreased while that of CO_2 increased.

In contrast to the activity of the catalysts described above, 10%Sn-TiO_2 catalyst is quite different. The lowest activity in steam reforming with a maximum conversion of 13.23% at 350 °C is observed for 10%Sn-TiO_2. This reaction had a low selectivity towards H_2, CO and CO_2. Methanation is highly favored with this catalyst with a maximum of 77.40% selectivity at 250 °C. It was observed by Bobadilla et al. [40] that Sn-based catalyst avoids the WGS reaction and has low catalytic activity. The low catalytic activity of 10%Sn-TiO_2 could be due to Sn metal particles in higher oxidation states and lower surface area. The SRM reaction of the catalyst was extremely slow and the run at 200 °C run could not be completed. Lastly, the 10%Zn-TiO_2 catalyst showed an increase in activity to 82.40% with an increase in temperature to 350 °C. The selectivity towards H_2 is 99% at all reaction temperatures and with low selectivity of CO with 1.19% at 350 °C. The Zn metal could have a unique interaction with the TiO_2 support creating a spinel-like structure confirmed by TPR, which are known to be thermally stable and resistance to coking. If all the different M-TiO_2 catalysts with 10 wt% were taken into account at 250 °C, the activity of the catalyst would go as follows: Sn< Cu< Zn< Co< Ni< Pd. Based on selectivity towards minimal CO, the Zn catalyst shows the lowest selectivity of 1.19%, with 97.84% conversion of methanol. Clearly, the Zn catalyst favors the WGS reaction and minimal methanol decomposition to produce CO. However, the concentration of CO is still quite high (> 10 ppm). As stated previously, the concentration of CO would have to be < 10 ppm to prevent poisoning of the Pt electrode in PEMFCs.

Table 4.4

Activity and selectivity of different M-TiO_2 catalysts for steam reforming of methanol

Catalyst	Temp (°C)	Conversion (%)	H_2 (%) Selectivity	CO (%) Selectivity	CH_4 (%) Selectivity	CO_2 (%) Selectivity
10%Co-TiO_2	200	10.98	94.66	45.91	8.21	45.88
	250	24.01	97.36	16.07	4.61	79.32
	300	42.37	96.81	8.20	6.14	85.66
	350	71.83	86.13	6.47	18.36	75.18
10%Ni-TiO_2	150	6.30	99.89	93.33	0.11	6.56
	200	12.61	99.57	94.08	0.43	5.49
	250	25.23	98.58	88.34	1.52	10.14
	300	44.94	97.56	83.36	2.52	14.12
	350	86.22	96.69	74.66	3.55	21.79
10%Cu-TiO_2	200	5.80	88.48	43.79	16.77	39.44
	250	14.48	96.72	56.39	5.19	38.42
	300	20.80	96.30	57.06	4.85	38.09
	350	28.22	91.04	72.00	9.22	18.78
10%Pd-TiO_2	150	8.04	99.55	76.01	0.50	23.48
	200	13.40	99.11	78.34	0.96	20.70
	250	43.83	98.10	78.60	2.03	19.37
	300	76.24	96.46	68.09	3.88	28.03
	350	97.84	93.71	33.51	7.66	58.83
10%Sn-TiO_2	250	1.72	35.61	11.05	77.40	11.55
	300	9.59	33.65	21.54	63.22	15.24
	350	13.23	51.6	24.37	47.20	28.43
10%Zn-TiO_2	200	5.42	99.71	7.93	1.84	90.24
	250	22.35	99.40	2.96	0.78	96.25
	300	65.66	99.77	1.53	0.34	98.13
	350	82.40	99.66	1.19	0.50	98.32

As Zn metal supported on titania exhibited lower selectivity towards CO, efforts were made to synthesize Zn-TiO_2 catalyst with 5, 15, and 20 wt% to reduce the selectivity towards CO even further down. Table 4.5 summarizes the steam reforming of methanol activity and selectivity of 5-20%Zn-TiO_2.

Table 4.5

Steam Reforming of Methanol activity and selectivity of 5-20%Zn-TiO_2 catalysts

Catalyst	Temp (°C)	Conversion (%)	H_2 Selectivity (%)	CO Selectivity (%)	CH_4 Selectivity (%)	CO_2 Selectivity (%)
5%Zn-TiO_2	200	5.64	99.09	9.28	1.36	89.36
	250	19.02	99.44	6.70	0.91	92.38
	300	28.13	99.70	2.44	0.44	97.11
	350	42.285	99.54	2.35	0.65	97.00
10%Zn-TiO_2	200	5.42	99.71	7.93	1.84	90.24
	250	22.35	99.40	2.96	0.78	96.25
	300	65.66	99.77	1.53	0.34	98.13
	350	82.40	99.66	1.19	0.50	98.32
15%Zn-TiO_2	200	5.95	99.41	4.69	0.84	94.47
	250	21.46	99.52	4.11	0.78	95.12
	300	67.79	99.43	1.74	0.81	97.45
	350	88.68	99.77	1.36	0.32	98.32
20%Zn-TiO_2	200	8.58	99.30	6.41	1.07	92.52
	250	14.86	99.25	4.71	1.24	94.05
	300	18.55	97.76	3.97	3.54	92.50
	350	29.01	99.08	2.19	1.18	96.62

All the 5-20%Zn-TiO_2 catalysts showed increasing activity with the increase in temperature. The catalytic activity improves as the metal loading increased from 5-15%. However, the catalytic activity drastically decreased when the loading was increased to 20%Zn-TiO_2. This is most likely due to the decrease in the specific surface area, in which the pores become larger. In all cases, the selectivity towards hydrogen is 99% and the selectivity of CO ranges from 1.19-9.28 %. The catalysts still promote the methanol decomposition and WGS reactions due to the by-products having higher selectivites towards H_2 and CO_2. The catalytic activity of Zn-TiO_2 catalyst goes as follows: 15Zn< 10Zn< 5Zn< 20Zn. Therefore, the surface area could be correlated to the catalytic activity, as higher the surface area of the Zn-TiO_2 the better is its catalytic activity.

CHAPTER 5

Conclusions and Future Work

5.1 Conclusions

Mesoporous-TiO_2 with high surface area was synthesized using a one-pot procedure in the presence of the surfactant, CTAB. The FTIR spectra showed the complete removal of the surfactant after calcination at 350 °C. The surface area of the catalysts was observed to increase with the addition of metals, except in the case of Pd metal. In the case of Pd, the surface area decreased due to the large PdO metal particles ~ 49.39 nm, causing a collapse in the mesoporous structure. N_2 adsorption-desorption isotherms and TEM studies confirmed that the material had a highly mesoporous nature even after the addition of metals. The wide angle XRD studied showed the existence of the catalytically active anatase phase. The intensity of the diffraction peaks was observed to decrease with the addition of metals onto the mesoporous support suggesting a decrease in crystallization. The decrease in crystallization led to the increase in surface area, which is a unique characteristic of mesoporous TiO_2. The TPR results showed the reduction behavior and temperature of the support and metal oxides. In some cases, two reduction steps could be observed for the catalyst. In the SRM reactions, the 10%Pd-TiO_2 and 10%Ni-TiO_2 catalysts showed activity for methanol reforming at as low as 150 °C. The 10%Pd-TiO_2 and 10%Ni-TiO_2 exhibited the highest catalytic activity in SRM reactions with methanol conversion of 97.84% and 86.22%, respectively at 350 °C. The 10%Cu-TiO_2 and 10%Sn-TiO_2 showed the lowest catalytic activity in SRM reactions. In overall, the steam reforming results suggest that the activity of the monometallic catalysts at 250 °C is as follows Pd>Ni>Co>Zn>Cu>Sn. The selectivity towards CO is as follows Zn<Co<Sn<Cu<Pd<Ni. The 10%Zn-TiO_2 catalyst showed the activity at 82.4%, H_2 selectivity at 99.66%, and the selectivity

towards CO with 1.19 % at a temperature of 350 °C. As for Zn-TiO_2 catalysts with different wt%, the 10%Zn-TiO_2 still showed the best results with low selectivity towards CO.

5.2 Future Work

Based on my research findings, I recommend the following for future work:

1. Optimization of one-pot synthesis of mesoporous TiO_2 catalysts: Different metals precipitate at different pH values. Therefore, in order to retain higher loading of each metal in mesoporous-TiO_2 support, it is important to study the effect of pH on the synthesis. The critical micelle concentration of the surfactant is very important in controlling the pore size and geometry of the mesoporous structure. A thorough understanding of the type and amount of the surfactant used during synthesis can play a significant role in the development of stable and robust catalyst.
2. Multimetallic TiO_2 Catalysts: According to SRM results, Pd exhibited the highest reactivity, whereas Zn and Co showed the lowest CO selectivity. The use of multi-metallic systems such as Pd-Zn-TiO_2, Pd-Co-TiO_2, and Pd-Zn-Co-TiO_2 are expected to promote a synergistic effect in reducing and/or eliminating the CO during SRM.

References

[1] A. J. Vizcaíno, A. Carrero, and J. A. Calles, "Hydrogen production by ethanol steam reforming over Cu–Ni supported catalysts," *International Journal of Hydrogen Energy*, vol. 32, pp. 1450-1461, 7// 2007.

[2] V. Nichele, M. Signoretto, F. Menegazzo, A. Gallo, V. Dal Santo, G. Cruciani, *et al*., "Glycerol steam reforming for hydrogen production: Design of Ni supported catalysts," *Applied Catalysis B: Environmental*, vol. 111–112, pp. 225-232, 1/12/ 2012.

[3] T.-C. Ou, F.-W. Chang, and L. S. Roselin, "Production of hydrogen via partial oxidation of methanol over bimetallic Au–Cu/TiO_2 catalysts," *Journal of Molecular Catalysis A: Chemical*, vol. 293, pp. 8-16, 10/1/ 2008.

[4] R. Perez-Hernandez, A. D. Avendano, E. Rubio, and V. Rodriguez-Lugo, "Hydrogen Production by Methanol Steam Reforming Over Pd/ZrO_2-TiO_2 Catalysts," *Topics in Catalysis*, vol. 54, pp. 572-578, Jun 2011.

[5] D. R. Palo, R. A. Dagle, and J. D. Holladay, "Methanol steam reforming for hydrogen production," *Chemical Reviews*, vol. 107, pp. 3992-4021, 2007.

[6] A. Taguchi and F. Schüth, "Ordered mesoporous materials in catalysis," *Microporous and Mesoporous Materials*, vol. 77, pp. 1-45, 1/3/ 2005.

[7] U. Ciesla and F. Schüth, "Ordered mesoporous materials," *Microporous and Mesoporous Materials*, vol. 27, pp. 131-149, 1999.

[8] Y. Ren, Z. Ma, and P. G. Bruce, "Ordered mesoporous metal oxides: synthesis and applications," *Chemical Society Reviews*, vol. 41, pp. 4909-4927, 2012.

[9] J. L. Vivero-Escoto, Y.-D. Chiang, K. C. Wu, and Y. Yamauchi, "Recent progress in mesoporous titania materials: adjusting morphology for innovative applications," *Science and Technology of Advanced Materials*, vol. 13, p. 013003, 2012.

[10] C. Song, "Fuel processing for low-temperature and high-temperature fuel cells: Challenges, and opportunities for sustainable development in the 21st century," *Catalysis Today*, vol. 77, pp. 17-49, 12/1/ 2002.

[11] J. N. Armor, "The multiple roles for catalysis in the production of H_2," *Applied Catalysis A: General*, vol. 176, pp. 159-176, 1/25/ 1999.

[12] L. F. Bobadilla, A. Álvarez, M. I. Domínguez, F. Romero-Sarria, M. A. Centeno, M. Montes, *et al*., "Influence of the shape of Ni catalysts in the glycerol steam reforming," *Applied Catalysis B: Environmental*, vol. 123–124, pp. 379-390, 7/23/ 2012.

[13] R. Pérez-Hernández, A. Gutiérrez-Martínez, J. Palacios, M. Vega-Hernández, and V. Rodríguez-Lugo, "Hydrogen production by oxidative steam reforming of methanol over $Ni/CeO_2–ZrO_2$ catalysts," *International Journal of Hydrogen Energy*, vol. 36, pp. 6601-6608, 6// 2011.

[14] V. Meynen, P. Cool, and E. F. Vansant, "Verified syntheses of mesoporous materials," *Microporous and Mesoporous Materials*, vol. 125, pp. 170-223, 10/15/ 2009.

[15] R. Zhang, A. A. Elzatahry, S. S. Al-Deyab, and D. Zhao, "Mesoporous titania: From synthesis to application," *Nano Today*, vol. 7, pp. 344-366, 8// 2012.

[16] T. Sreethawong and S. Yoshikawa, "Enhanced photocatalytic hydrogen evolution over Pt supported on mesoporous TiO_2 prepared by single-step sol–gel process with surfactant template," *International journal of hydrogen energy*, vol. 31, pp. 786-796, 2006.

[17] E. A. Kozlova and A. V. Vorontsov, "Influence of mesoporous and platinum-modified titanium dioxide preparation methods on photocatalytic activity in liquid and gas phase," *Applied Catalysis B: Environmental*, vol. 77, pp. 35-45, 2007.

[18] M. Singh, S. Manikandan, and A. Kumaraguru, "Nanoparticles: A new technology with wide applications," *Res. J. Nanosci. Nanotechnol,* vol. 1, pp. 1-11, 2011.

[19] L. L. Hench and J. K. West, "The sol-gel process," *Chemical Reviews,* vol. 90, pp. 33-72, 1990.

[20] X. Chen and S. S. Mao, "Titanium dioxide nanomaterials: synthesis, properties, modifications, and applications," *Chemical reviews,* vol. 107, pp. 2891-2959, 2007.

[21] D. M. Antonelli and J. Y. Ying, "Mesoporous materials," *Current Opinion in Colloid & Interface Science,* vol. 1, pp. 523-529, 8// 1996.

[22] D. M. Antonelli, "Synthesis of phosphorus-free mesoporous titania via templating with amine surfactants," *Microporous and Mesoporous Materials,* vol. 30, pp. 315-319, 9// 1999.

[23] N. N. Madikizela-Mnqanqeni and N. J. Coville, "The preparation and study of sol–gel synthesized Co/Zn/TiO_2 Fischer–Tropsch catalysts," *Applied Catalysis A: General,* vol. 317, pp. 195-203, 2007.

[24] D. W. Lee and B. R. Yoo, "Advanced metal oxide (supported) catalysts: Synthesis and Applications," *Journal of Industrial and Engineering Chemistry,* 2014.

[25] C. J. Brinker, Y. Lu, A. Sellinger, and H. Fan, "Evaporation-induced self-assembly: nanostructures made easy," *Advanced materials,* vol. 11, pp. 579-585, 1999.

[26] G. d. A. Soler-Illia, A. Louis, and C. Sanchez, "Synthesis and characterization of mesostructured titania-based materials through evaporation-induced self-assembly," *Chemistry of Materials,* vol. 14, pp. 750-759, 2002.

[27] S. R. Gajjela, K. Ananthanarayanan, C. Yap, M. Gratzel, and P. Balaya, "Synthesis of mesoporous titanium dioxide by soft template based approach: characterization and

application in dye-sensitized solar cells," *Energy & Environmental Science*, vol. 3, pp. 838-845, Jun 2010.

[28] M. Mihaylov, K. Hadjiivanov, N. Abadjieva, D. Klissurski, and L. Mintchev, "Characterization of zirconia-supported nickel catalysts prepared by multiple ion-exchange," *Studies in Surface Science and Catalysis*, vol. 118, pp. 295-304, 1998.

[29] D. Zhao, P. Yang, N. Melosh, J. Feng, B. F. Chmelka, and G. D. Stucky, "Continuous mesoporous silica films with highly ordered large pore structures," *Advanced Materials*, vol. 10, pp. 1380-1385, 1998.

[30] S. S. Bhoware and A. Singh, "Characterization and catalytic activity of cobalt containing MCM-41 prepared by direct hydrothermal, grafting and immobilization methods," *Journal of Molecular Catalysis A: Chemical*, vol. 266, pp. 118-130, 2007.

[31] J. Jin, J. Ouyang, and H. Yang, "One-step synthesis of highly ordered Pt/MCM-41 from natural diatomite and the superior capacity in hydrogen storage," *Applied Clay Science*, vol. 99, pp. 246-253, 2014.

[32] L.-C. Wang, C.-Y. Huang, C.-Y. Chang, W.-C. Lin, and K.-J. Chao, "Formation of Pd nanoparticles in surfactant-mesoporous silica composites and surfactant solutions," *Microporous and Mesoporous Materials*, vol. 110, pp. 451-460, 2008.

[33] H. Jiang, H. Bongard, W. Schmidt, and F. Schüth, "One-pot synthesis of mesoporous Cu–γ-Al_2O_3 as bifunctional catalyst for direct dimethyl ether synthesis," *Microporous and Mesoporous Materials*, vol. 164, pp. 3-8, 2012.

[34] A. Prabhu, A. Al Shoaibi, and C. Srinivasakannan, "Synthesis and characterization of mesoporous carbon by simple one pot method," *Materials Letters*, vol. 136, pp. 81-84, 2014.

[35] J. M. Campelo, D. Luna, R. Luque, J. M. Marinas, and A. A. Romero, "Sustainable preparation of supported metal nanoparticles and their applications in catalysis," *ChemSusChem,* vol. 2, pp. 18-45, 2009.

[36] S. Sá, H. Silva, L. Brandão, J. M. Sousa, and A. Mendes, "Catalysts for methanol steam reforming—A review," *Applied Catalysis B: Environmental,* vol. 99, pp. 43-57, 8/31/ 2010.

[37] Y. Liu, T. Hayakawa, T. Tsunoda, K. Suzuki, S. Hamakawa, K. Murata, *et al*., "Steam reforming of methanol over Cu/CeO_2 catalysts studied in comparison with Cu/ZnO and Cu/Zn (Al) O catalysts," *Topics in catalysis,* vol. 22, pp. 205-213, 2003.

[38] N. Iwasa, T. Mayanagi, W. Nomura, M. Arai, and N. Takezawa, "Effect of Zn addition to supported Pd catalysts in the steam reforming of methanol," *Applied Catalysis A: General,* vol. 248, pp. 153-160, 8/8/ 2003.

[39] N. Iwasa, S. Masuda, N. Ogawa, and N. Takezawa, "Steam reforming of methanol over Pd/ZnO: Effect of the formation of PdZn alloys upon the reaction," *Applied Catalysis A: General*, vol. 125, pp. 145-157, 4/27/ 1995.

[40] L. F. Bobadilla, S. Palma, S. Ivanova, M. I. Domínguez, F. Romero-Sarria, M. A. Centeno, *et al*., "Steam reforming of methanol over supported Ni and Ni–Sn nanoparticles," *International Journal of Hydrogen Energy,* vol. 38, pp. 6646-6656, 5/30/ 2013.

[41] R. Pérez-Hernández, G. Mondragón Galicia, D. Mendoza Anaya, J. Palacios, C. Angeles-Chavez, and J. Arenas-Alatorre, "Synthesis and characterization of bimetallic Cu–Ni/ZrO_2 nanocatalysts: H_2 production by oxidative steam reforming of methanol," *International Journal of Hydrogen Energy,* vol. 33, pp. 4569-4576, 9// 2008.

[42] J. L. Contreras, J. Salmones, J. A. Colín-Luna, L. Nuño, B. Quintana, I. Córdova, *et al*., "Catalysts for H_2 production using the ethanol steam reforming (a review)," *International Journal of Hydrogen Energy*.

[43] H. Song, L. Zhang, R. B. Watson, D. Braden, and U. S. Ozkan, "Investigation of bio-ethanol steam reforming over cobalt-based catalysts," *Catalysis Today*, vol. 129, pp. 346-354, 12/15/ 2007.

[44] M. S. Batista, R. K. S. Santos, E. M. Assaf, J. M. Assaf, and E. A. Ticianelli, "High efficiency steam reforming of ethanol by cobalt-based catalysts," *Journal of Power Sources*, vol. 134, pp. 27-32, 7/12/ 2004.

[45] S. Liguori, A. Iulianelli, F. Dalena, V. Piemonte, Y. Huang, and A. Basile, "Methanol steam reforming in an Al_2O_3 supported thin Pd-layer membrane reactor over $Cu/ZnO/Al_2O_3$ catalyst," *International Journal of Hydrogen Energy*.

[46] S. Liu, K. Takahashi, H. Eguchi, and K. Uematsu, "Hydrogen production by oxidative methanol reforming on Pd/ZnO: Catalyst preparation and supporting materials," *Catalysis Today*, vol. 129, pp. 287-292, 12/15/ 2007.

[47] F. Pinzari, P. Patrono, and U. Costantino, "Methanol reforming reactions over Zn/TiO_2 catalysts," *Catalysis Communications*, vol. 7, pp. 696-700, 9// 2006.

[48] M. Arsalanfar, A. A. Mirzaei, H. R. Bozorgzadeh, H. Atashi, S. Shahriari, and A. Pourdolat, "Structural characteristics of supported cobalt–cerium oxide catalysts used in Fischer–Tropsch synthesis," *Journal of Natural Gas Science and Engineering*, vol. 9, pp. 119-129, 11// 2012.

[49] S. Janitabar Darzi, A. R. Mahjoub, and A. Nilchi, "Synthesis of Spongelike Mesoporous Anatase and its Photocatalytic Properties," *Iran. J. Chem. Chem. Eng. Vol*, vol. 29, 2010.

[50] A.-C. Lee, R.-H. Lin, C.-Y. Yang, M.-H. Lin, and W.-Y. Wang, "Preparations and characterization of novel photocatalysts with mesoporous titanium dioxide TiO_2 via a sol–gel method," *Materials Chemistry and Physics*, vol. 109, pp. 275-280, 2008.

[51] N. Alexaki, T. Stergiopoulos, A. G. Kontos, D. S. Tsoukleris, A. P. Katsoulidis, P. J. Pomonis, *et al*., "Mesoporous titania nanocrystals prepared using hexadecylamine surfactant template: Crystallization progress monitoring, morphological characterization and application in dye-sensitized solar cells," *Microporous and Mesoporous Materials*, vol. 124, pp. 52-58, Aug-Sep 2009.

[52] K. S. Sing, "Reporting physisorption data for gas/solid systems with special reference to the determination of surface area and porosity (Recommendations 1984)," *Pure and applied chemistry*, vol. 57, pp. 603-619, 1985.

[53] M. H. Youn, J. G. Seo, and I. K. Song, "Hydrogen production by auto-thermal reforming of ethanol over nickel catalyst supported on metal oxide-stabilized zirconia," *International Journal of Hydrogen Energy*, vol. 35, pp. 3490-3498, 4// 2010.

[54] H. Chen, K. Dai, T. Peng, H. Yang, and D. Zhao, "Synthesis of thermally stable mesoporous titania nanoparticles via amine surfactant-mediated templating method," *Materials chemistry and physics*, vol. 96, pp. 176-181, 2006.

[55] L. G. Teoh, Y.-C. Lee, Y. S. Chang, T.-H. Fang, and H. M. Chen, "Preparation and characterization of nanocrystalline titanium dioxide with a surfactant-mediated method," *Current Nanoscience*, vol. 6, pp. 77-81, 2010.

[56] H. Q. Zhu, Z. F. Qin, W. J. Shan, W. J. Shen, and J. G. Wang, "Pd/CeO_2-TiO_2 catalyst for CO oxidation at low temperature: a TPR study with H_2 and CO as reducing agents," *Journal of Catalysis*, vol. 225, pp. 267-277, Jul 25 2004.

[57] A. Vizcaino, A. Carrero, and J. Calles, "Pure silica SBA-15 supported Cu-Ni catalysts for hydrogen production by ethanol steam reforming," in *Proceedings of 16th World Hydrogen Energy Conference, Lyon, France*, 2006.

[58] Y. Matsumura, "Enhancement in activity of Pd–Zn catalyst for methanol steam reforming by coprecipitation on zirconia support," *Applied Catalysis A: General,* vol. 468, pp. 350-358, 11/5/ 2013.

[59] Y.-M. Lu, C.-Y. Chen, and M. H. Lin, "Effect of hydrogen plasma treatment on the electrical properties of sputtered N-doped cuprous oxide films," *Thin Solid Films,* vol. 480–481, pp. 482-485, 6/1/ 2005.

[60] V. Nichele, M. Signoretto, F. Menegazzo, I. Rossetti, and G. Cruciani, "Hydrogen production by ethanol steam reforming: Effect of the synthesis parameters on the activity of Ni/TiO_2 catalysts," *International Journal of Hydrogen Energy,* vol. 39, pp. 4252-4258, 3/18/ 2014.

[61] J. Xiaoyuan, D. Guanghui, L. Liping, C. Yingxu, and Z. Xiaoming, "Catalytic activities of CuO/TiO_2 and $CuO\text{-}ZrO_2/TiO_2$ in NO + CO reaction," *Journal of Molecular Catalysis A: Chemical,* vol. 218, pp. 187-195, 8/24/ 2004.

[62] K.-R. Hwang, S.-K. Ihm, S.-C. Park, and J.-S. Park, "Pt/ZrO_2 catalyst for a single-stage water-gas shift reaction: Ti addition effect," *International Journal of Hydrogen Energy,* vol. 38, pp. 6044-6051, 5/10/ 2013.

[63] M. Hosseini, S. Siffert, H. L. Tidahy, R. Cousin, J. F. Lamonier, A. Aboukais, *et al*., "Promotional effect of gold added to palladium supported on a new mesoporous TiO_2 for total oxidation of volatile organic compounds," *Catalysis Today,* vol. 122, pp. 391-396, 4/30/ 2007.

[64] H. L. Tidahy, S. Siffert, J. F. Lamonier, E. A. Zhilinskaya, A. Aboukaïs, Z. Y. Yuan, *et al*., "Characterisation of new Pd/hierarchical macro-mesoporous ZrO_2, TiO_2, and ZrO_2-TiO_2 catalysts for toluene total oxidation," in *Studies in Surface Science and Catalysis*. vol. Volume 160, F. R.-R. J. R. P.L. Llewellyn and N. Seaton, Eds., ed: Elsevier, 2007, pp. 201-208.

[65] I. Eswaramoorthi and A. K. Dalai, "A comparative study on the performance of mesoporous SBA-15 supported Pd–Zn catalysts in partial oxidation and steam reforming of methanol for hydrogen production," *International Journal of Hydrogen Energy*, vol. 34, pp. 2580-2590, 3// 2009.

[66] I. Rossetti, J. Lasso, E. Finocchio, G. Ramis, V. Nichele, M. Signoretto, *et al*., "TiO_2-supported catalysts for the steam reforming of ethanol," *Applied Catalysis A: General*, vol. 477, pp. 42-53, 5/5/ 2014.

[67] M. L. Smith, A. Campos, and J. J. Spivey, "Reduction processes in Cu/SiO_2, Co/SiO_2, and $CuCo/SiO_2$ catalysts," *Catalysis Today*, vol. 182, pp. 60-66, 2012.

[68] B. Bayram, I. I. Soykal, D. von Deak, J. T. Miller, and U. S. Ozkan, "Ethanol steam reforming over Co-based catalysts: Investigation of cobalt coordination environment under reaction conditions," *Journal of Catalysis*, vol. 284, pp. 77-89, Nov 1 2011.

[69] X. Meng, H. Huang, H. X. Weng, and L. Shi, "Ni/ZnO-based Adsorbents Supported on Al_2O_3, SiO_2, TiO_2, ZrO_2: A Comparison for Desulfurization of Model Gasoline by Reactive Adsorption," *Bulletin of the Korean Chemical Society*, vol. 33, pp. 3213-3217, Oct 20 2012.

[70] A. Vita, L. Pino, F. Cipiti, M. Lagana, and V. Recupero, "Biogas as renewable raw material for syngas production by tri-reforming process over $NiCeO_2$ catalysts: Optimal

operative condition and effect of nickel content," *Fuel Processing Technology*, vol. 127, pp. 47-58, Nov 2014.

[71] S. Hull and J. Trawczynski, "Steam reforming of ethanol on zinc containing catalysts with spinel structure," *International Journal of Hydrogen Energy*, vol. 39, pp. 4259-4265, Mar 18 2014.

[72] J. Li, P. Zhao, and S. Liu, "SnOx–MnOx–TiO_2 catalysts with high resistance to chlorine poisoning for low-temperature chlorobenzene oxidation," *Applied Catalysis A: General*, vol. 482, pp. 363-369, 7/22/ 2014.

[73] N. Nava and T. Viveros, "Structural studies of supported tin catalysts," *Hyperfine Interactions*, vol. 122, pp. 147-153, 1999.

[74] D. A. Kumar, J. M. Shyla, and F. P. Xavier, "Synthesis and characterization of TiO_2/SiO_2 nano composites for solar cell applications," *Applied Nanoscience*, vol. 2, pp. 429-436, 2012.

[75] N. Khalid, E. Ahmed, M. Ikram, M. Ahmad, D. Phoenix, A. Elhissi, *et al*., "Effects of Calcination on Structural, Photocatalytic Properties of TiO_2 Nanopowders Via $TiCl_4$ Hydrolysis," *Journal of materials engineering and performance*, vol. 22, pp. 371-375, 2013.

Appendix A

Thermo gravimetric analysis-differential calorimetry of (1) 10%Cu-TiO_2 (2) 10%Sn-TiO_2

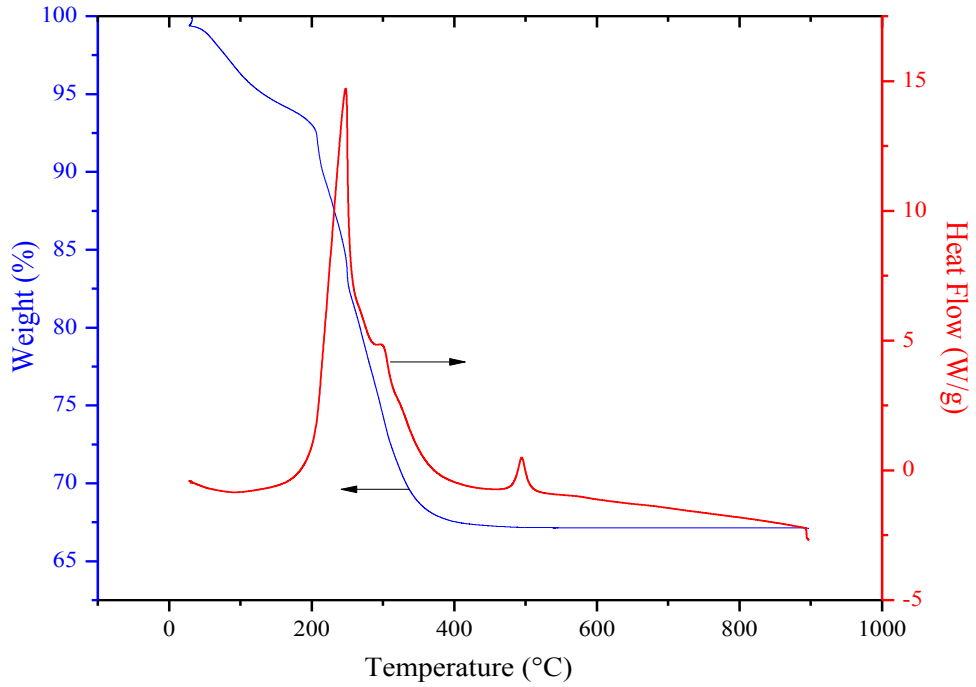

(1)

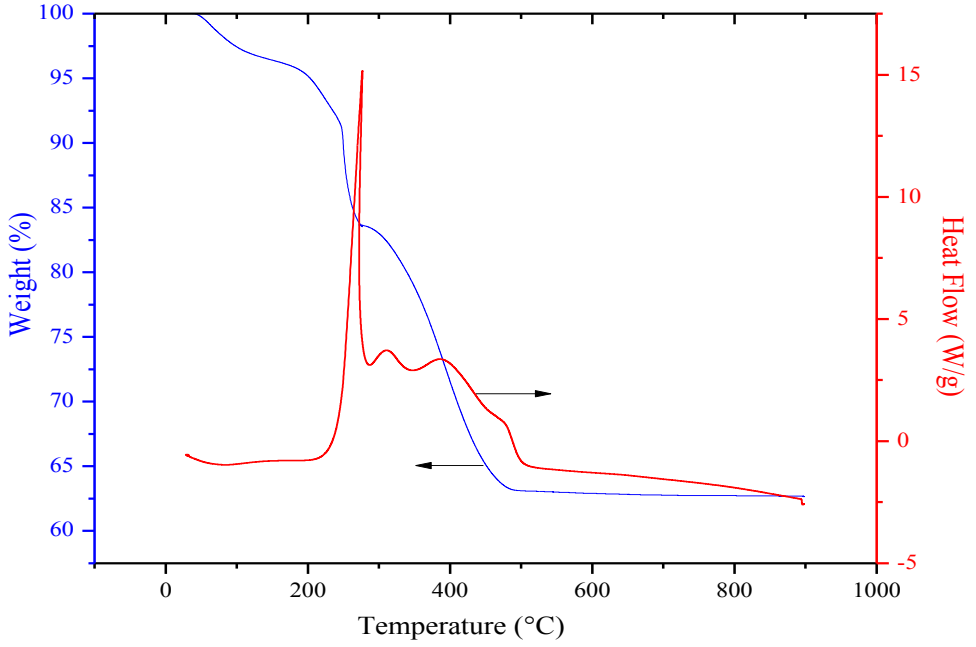

(2)

For peak descriptions, see section **4.1.1.**

Appendix B

Experimental Calculations

Synthesis of 5 g 10% Ni-TiO_2

Composition of the catalyst: 10% Ni
90% TiO_2

Amount of metal in the catalyst (g):

$$\frac{Amount\ of catalyst\ to\ be\ prepared\ (g)\ X\ Composition\ of\ metal\ in\ catalyst\ (\%)}{100}$$

(5 g) X (10%) / 100 = 0.5 g of $Ni(NO_3)_2$. $6H_2O$

Amount of TiO_2 in the catalyst (g):

$$\frac{Amount\ of\ catalyst\ to\ be\ prepared\ (g)\ X\ Composition\ of\ TiO_2\ in\ catalysts\ (\%)}{100}$$

(5g) X (90%) /100 = 4.5 g of TiO_2

MOLE RATIO: 1 TIPR: 0.52 CTAB: 282 H_2O: 26.21 ethanol

1 mole of TiO_2 = 1 mole of TIPR, therefore 79.86 g of TiO_2 = 284.22 g of TIPR

Amount of TIPR to be used to get required 4.5 g of TiO_2 (g):

$$\frac{Amount of\ TiO_2\ in\ the catalyst(g)\ X\ MW\ of\ TIPR\ (g/mol)}{MW\ of\ TiO_2\ (g/mol)}$$

(4.5 g) x (284.22 g/mol) / (79.86 g/mol) = 16.02 g of TIPR

Volume of TIPR used (mL): $\frac{Amount of\ TIPR\ to\ be\ used\ to\ get\ required TIPR\ (g)}{Density of\ TIPR\ (g/mL)}$

(16.02 g) / (0.95 g/mL) = **16.86 mL of TIPR**

Actual quantities of TIPR used in moles: $\frac{Amount\ of\ TIPR\ used\ (g)}{MW\ of\ TIPR\ (g/mol)}$

(16.02 g) / (284.22 g/mol) = 0.056 mol of TIPR

1 mole of metal = 1 mole of metal precursor, **t**herefore 58.69 g of metal = 290.79 g metal precursor

Amount of metal to be used:

$$\frac{Amount\ of\ metal\ in\ the\ catalyst(g)}{MW\ of\ metal(g/mol)}\ X\ MW\ of\ precursors(g/mol)$$

((0.5g) / (58.69 g/mol) X 290.60 g/mol) = **2.477 g of $Ni(NO_3)_2$. $6H_2O$**

Actual quantities of metal used in moles: $\frac{Actual\ quantities\ used\ (g)}{MW\ of\ metal\ precursors(g/mol)}$

(2.477 g) / (290.79 g/mol) = 0.0085 mol of $Ni(NO_3)_2$. $6H_2O$

Actual quantities of H_2O used in moles:

$$Actual\ quantities\ of\ TIPR\ used\ (mol)\ X\ Composition\ of\ H_2O\ used$$

(0.056 mol) X (282) = 15.89 mol of H_2O

Actual quantities of H_2O used in g: $Actual\ quantities\ used\ (mol)\ X\ MW\ of\ H_2O\ (g/mol)$

(15.89 mol) X (18 g/mol) = 286.03 g of H_2O

Actual quantities of H_2O used (mL): $\frac{Actual\ quantities\ used\ (g)}{Density\ of\ H_2O\ (g/mL)}$

(286.03 g) / (1 g/mL) = **286.03 mL of H_2O**

Actual quantities of CTAB used in moles:

$$Actual\ quantities\ of\ TIPR\ used\ (mol)\ X\ Composition\ used\ (molar\ ratio)$$

(0.056 mol) X (0.52) = 0.029 mol of CTAB

Actual quantities of CTAB used in g:

$$Actual\ quantities\ of\ CTAB\ used\ (mol)\ X\ MW\ of\ CTAB\ (g/mol)$$

(0.029 mol) X (364.44 g/mol) = **10. 68 g of CTAB**

Actual quantities of ethanol: $\frac{Actual quantities of\ H_2O\ used (mL)}{4}$

(286.03 mL / 4) = **71.5 mL of ethanol**

Actual quantities of ethanol used (g):

$$Actual\ quanties\ used\ (mL)\ X\ Density\ of\ TIPR\ (g/mL)$$

(71.5 mL) X (0.95 g/mL) = 67.93 g of ethanol

Actual quantities of ethanol used in moles: $\frac{Actual quantities of\ ethanol used (g)}{MW\ of\ ethanol (g/mol)}$

(67.93 g) / (46 g/mol) = 1.48 mol of ethanol

Composition of ethanol used in mole ratio:

$$\frac{Actual quantities of\ ethanol used (mol)}{Actual quantities of\ TIPR\ used (mol)}$$

(1.48 mol) / (0.056 mol) = 26.21

Typical Weights for 5 g of catalysts

Catalysts	CTAB (g)	H_2O (mL)	EtOH (mL)	TIPR (mL)	$Pd(NO_3)_2$ (g)	$Zn(NO_3)_2$ (g)	$Cu(NO_3)_2$ (g)	$Ni(NO_3)_2$ (g)	$SnCl_2$ (g)	$CoCl_2$ (g)
TiO_2	11.87	317	79.45	18.73	-	-	-	-	-	-
10%Co-TiO_2	10.68	286	71.5	16.86	-	-	-	-	-	2.09
10%Cu-TiO_2	10.68	286	71.5	16.86	-	-	1.83	-	-	-
10%Sn-TiO_2	10.68	286	71.5	16.86	-	-	-	-	0.95	-
10%Pd-TiO_2	10.68	286	71.5	16.86	1.17	-	-	-	-	-
10%Ni-TiO_2	10.68	286	71.5	16.86	-	-	-	2.58	-	-
5%Zn-TiO_2	11.27	302	75.48	17.79	-	1.14	-	-	-	-
10%Zn-TiO_2	10.68	286	71.50	16.86	-	2.27	-	-	-	-
15%Zn-TiO_2	10.09	270	67.53	15.13	-	3.41	-	-	-	-
20%Zn-TiO_2	9.49	254	63.56	14.98	-	4.55	-	-	-	-

Appendix C

Gas Chromatography Calculations

Methanol/Water (1/3) Feed Calculations

Molecular weight of Methanol =	32	g/mol
Molecular weight of water =	18	g/mol
Density of Methanol =	0.792	g/mL
Density of water =	1	g/mL
Amt of methanol used in mL =	**40**	mL
Amt of methonl used in g =	31.68	g
Amt of methanol in moles =	0.99	moles
Methanol:Water molar ratio to be used = **1 :**	**3**	
Amt of water to be used in moles =	2.97	moles
Amt of water to be used in g =	53.46	g
Amt of water to be used in mL =	**53.46**	mL
Total volume of the solution =	**93.46**	mL
Concentration of the methanol =	**0.338968543**	g/mL
Concentration of water in solution =	0.572009416	g/mL

Gas hour space velocity calculations

Methanol concentration=	0.3389	g/mL
Water concentration =	0.572	g/mL
Total Flow	0.137	mL/min
(for 0.2 mL flow setting on pump)		
Methanol =	0.0464293	g/min
	2.785758	g/hr
water =	0.078364	g/min
	4.70184	g/hr
Moles of methanol =	0.087054938	mol/hr
Moles of water =	0.261213333	mol/hr
P=	101325	Pa
T =	298	K
R=	8.314	Pa. m^3/(K. mol)
PV=nRT		
V methanol=	0.002128644	m^3/hr
	2.12864422	lit/hr
V water =	0.006387119	m^3/hr
	6.387119079	lit/hr
Total feed flow =	8515.763299	mL/hr
Volume of the reactor =	3	mL
GHSV =	**2838.587766**	/hr

Typical GC Chromatogram

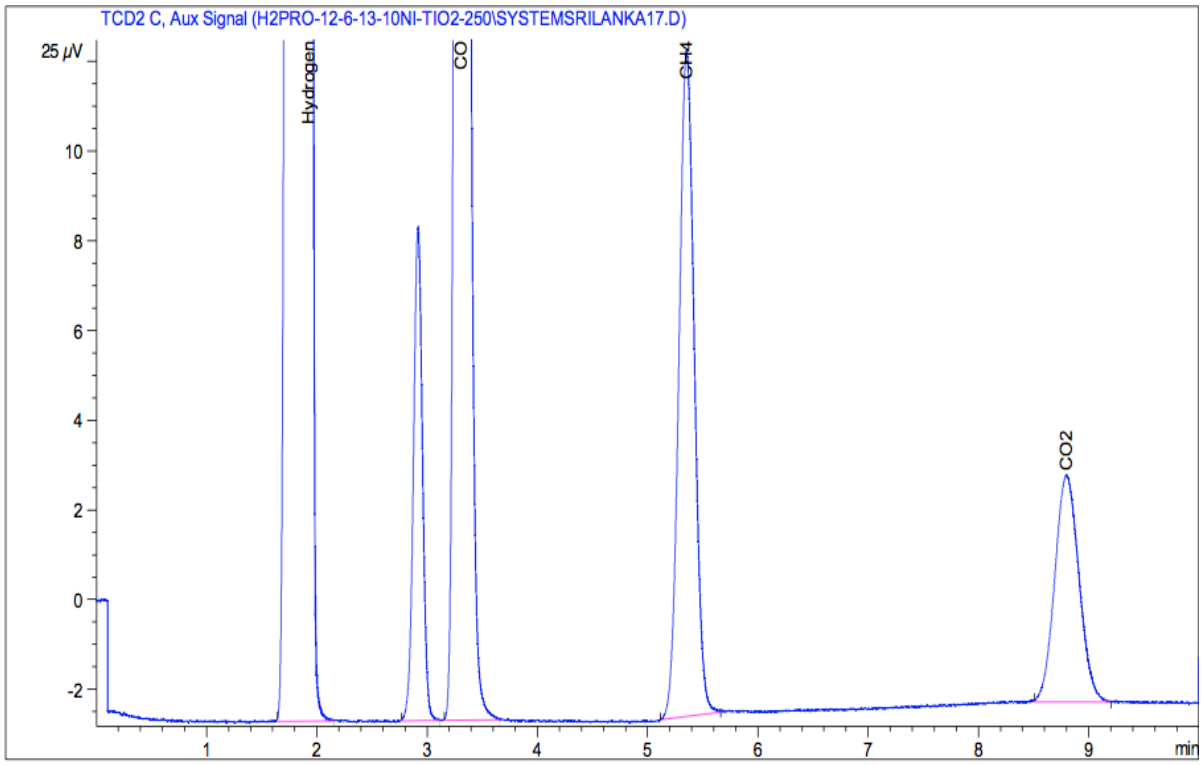


```
=========================================================================
                        External Standard Report
=========================================================================

Sorted By             :      Signal
Calib. Data Modified  :      11/7/2013 12:17:44 PM
Multiplier            :      1.0000
Dilution              :      1.0000
Do not use Multiplier & Dilution Factor with ISTDs

Signal 1: TCD2 C, Aux Signal

RetTime  Type      Area      Amt/Area    Amount    Grp   Name
 [min]          [25 µV*s]              [% (mol)]
-------|------|----------|----------|----------|--|------------------
  1.920 BB     8737.86035 3.55193e-3   31.03631    Hydrogen
  3.302 BB      604.49377 2.05082e-2   12.39709    CO
  5.351 BB      143.17456 5.97167e-3 8.54992e-1    CH4
  8.796 BB       76.98527 2.04745e-2    1.57623    CO2

Totals :                                45.86462
```

For GC operating parameters, see Table 3.2.

Appendix D

Standard Operating Procedure for the NOVA 2200e BET Instrument

Sample Cell Calibration Procedure

The individual sample cell must be calibrated before the analysis. This needs to be conducted for each (Sample Cell + Filler rod + Station) combination. Each combination will be given a unique cell number. This will be done only once for each combination and it will be automatically saved in the floppy disk of the instrument so no need to do it again until the floppy disk in the instrument has been formatted or changed. This calibration is essentially a 25-point blank analysis (i.e. without sample). Up to 99 cell calibrations can be saved per user disc. During a sample analysis, the NOVA program refers to this file. It is very important to use the correct cell calibrations with the cells that are actually used; otherwise, differences in volumes will result in erroneous data.

1. To perform a cell calibration using NOVAWin2 select **Operation** and click **Calibrate Cell** from the drop-down submenu which will open the following window (**Figure 1**).

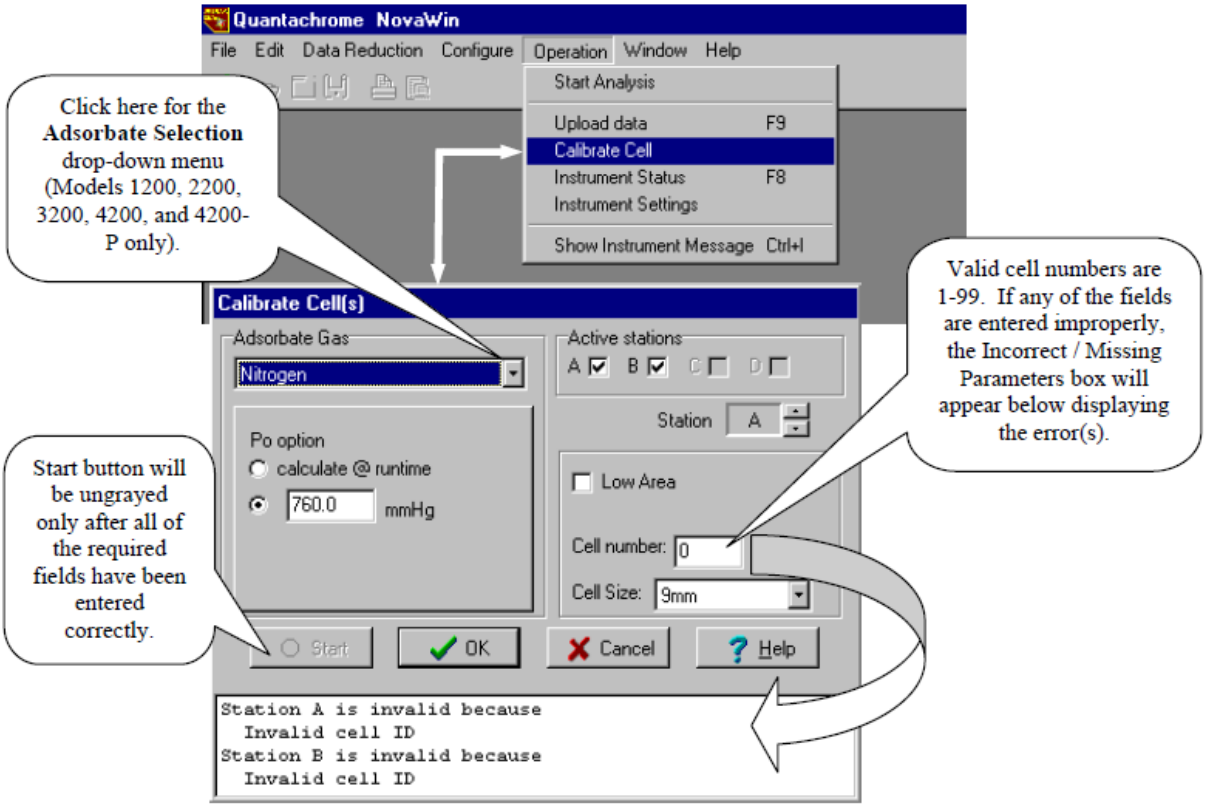

Figure 1

2. Select the station for the calibration. The distinction should be made as to which cell is in each station in that cells of different sizes may be calibrated together during a cell calibration.
3. Choose a P_0 option. The recommended value for P_0 is "Calculate at Run Time"
4. Enter a unique **Cell Number** to identify the particular sample cell. This number is associated with a certain combination of (sample cell+ filler rod + Station). Once the calibration is performed on a cell, the operator has to invoke the appropriate cell number at analysis time.
5. Select the **Cell Size** of the sample cell to be calibrated.
6. Choose the **Adsorbate** for the cell, Nitrogen is the defaulted selection.
7. Click the start button to begin the calibration.
8. Follow the same procedure to calibrate all the cells with unique rod and station combination.

Outgassing Procedure:

The Outgassing of the sample is done to remove all the adsorbed moisture or other gases before doing the BET analysis. Outgassing of the sample on NOVA 2200e can be done only using the instrument from control panel and not using the Novawin software.

1. Weight the dry and clean empty sample cell and note down the weight. Put the amount of catalyst sample (which will have roughly 10-15 m^2) of surface area, place the sample cell in the pouch of the heating mantle, set clamp in place, insert cell into fitting and tighten the fitting.
2. To start the Outgassing, go to the **Home Screen ➔ Control Panel ➔ Degas Stations ➔ Press appropriate number** to load the sample.
3. To test the sample for complete outgassing, go to **Home Screen ➔ Control Panel ➔** Manual Mode ➔ press appropriate numbers to open **Valve 4** and **valve 2** (Valve 3 and Valve 6 will already be open during outgassing)**,** so now four valves i.e. 6, 3, 4, 2 will be open that is called evacuation of the sample line. Monitor the pressure reading on the screen and wait to get it constant. Once it is constant close valve 4 & 3 and open valve 2. Again monitor the pressure on the screen (pressure will increase slightly with time). If the change in pressure is less than 0.03 mmHg/min your outgassing is complete. If it is above

0.03 mmHg you need to keep the sample outgassing for some more time and do the outgassing test again to check.

4. Once the Outgassing is done, go to the **Home Screen ➔ Control Panel ➔ Degas Stations ➔ Press appropriate number** to unload the sample
5. Measure the weight of the sample cell with the outgassed sample and subtract the weight of the empty sample cell to get exact weigh of the dried catalyst sample which will be using in next stage of analysis.

Analysis Procedure

1. Fill the dewar flask with the liquid nitrogen and place and place it firmly in the analysis chamber and place the outgassed sample cell to the analysis station.
2. To begin the analysis, select **operation ➔ Start Analysis** as shown in **Figure 2**.

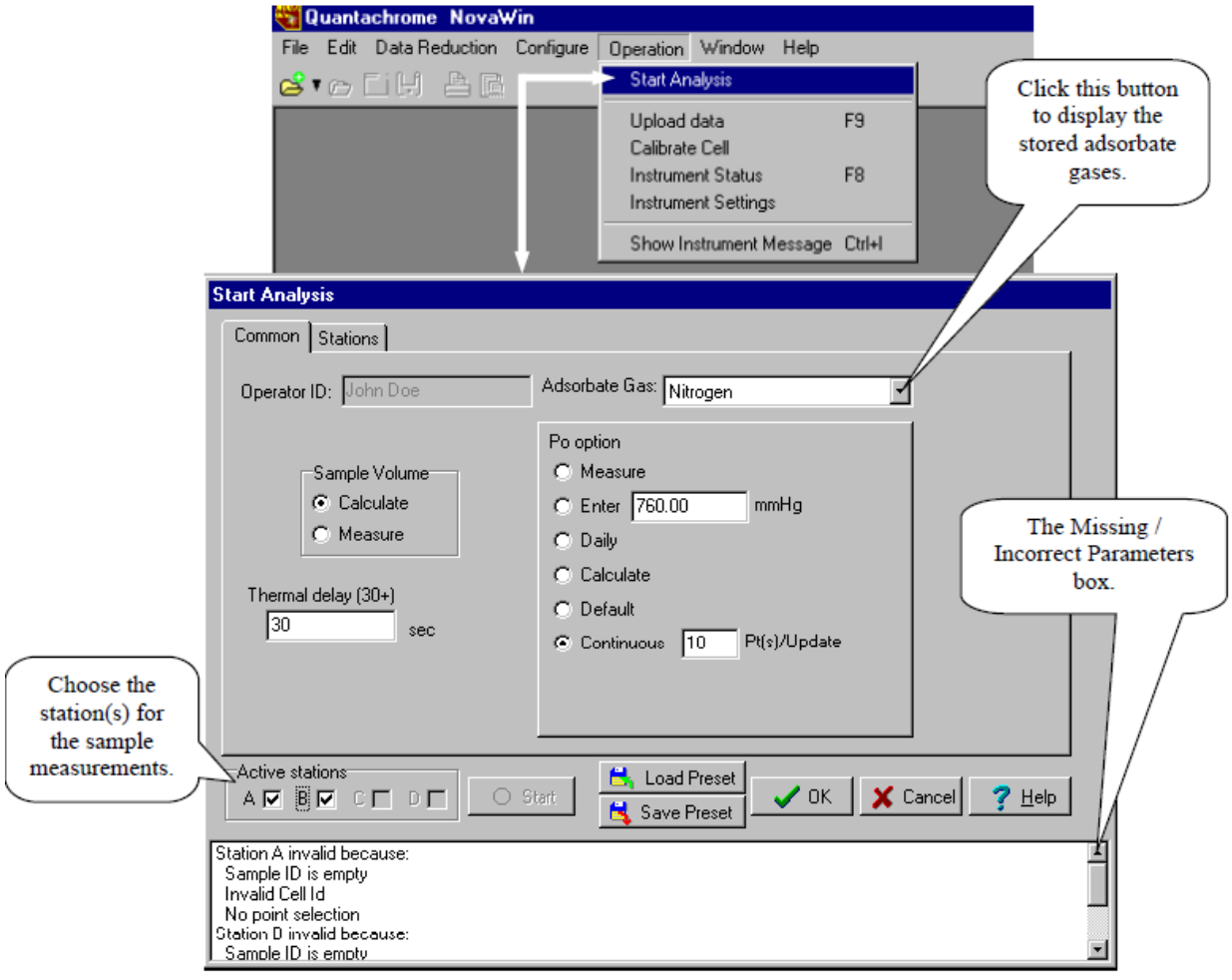

Figure 2

The Analysis Setup window consists of two parts: the **Common Tab** and the **Stations Tab**. The Common tab is where the parameters are set for the measurements that are common to all of the sample cells for the analysis (adsorbate selection, P_0 determination, thermal delay, and sample volume determination, if desired). The Stations tab in the Analysis Setup window is where parameters such as specific sample information (sample identification and sample weight), data point selection, and equilibrium criteria can be set for each of the individual stations.

3. In the **Common** tab (**Figure 2**), enter **your name** as **Operator ID**, Select **Nitrogen** as an **Adsorbate Gas**, and enter **180 sec** for **Thermal delay (30+)** option
4. For the **P_0 Option** choose **Calculate** where at the beginning of an analysis, the manifold is pressurized and atmosphere is measured in the manifold. The value measured is ambient pressure and 10 mm Hg is added to that value.

5. Check the **Measure** option box in the **Sample Volume** so that NOVA will measure the volume of the sample in case the density of the sample is not known (which is the case most of the time for our analysis).

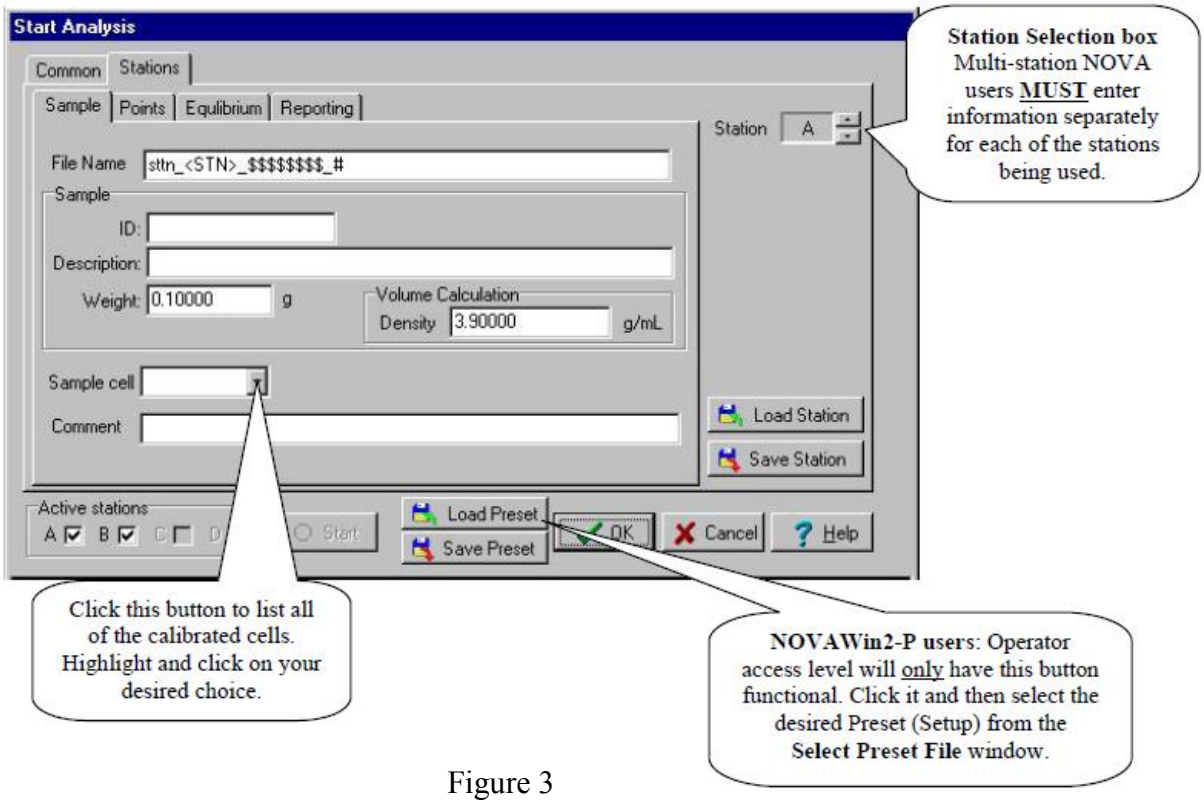

Figure 3

6. In the **Station** tab ➔ **Sample** tab (**Figure 3**); enter File Name (for your reference), ID, description and Weight of the sample. The **Density** option will be inactive as we chose **Measure** option for the sample volume in Common tab due to unknown density.
7. Select the Sample cell number which was calibrated for each cell + rod + station combination from the dropdown list.
8. Check the box for the active station either A or B or both A & B.
9. In the **Station** tab ➔ **Points** tab, (here the data points for the measurements are selected for each of the stations in the Analysis Setup parameters), load the 11 point, 26 or 48 point analysis file from **Load Point** option which is developed in house according to the need of surface area measurement (11 pts is enough) and detail measurements (like surface area, pore size and pore volume, 26 or 48 pt analysis will be good)

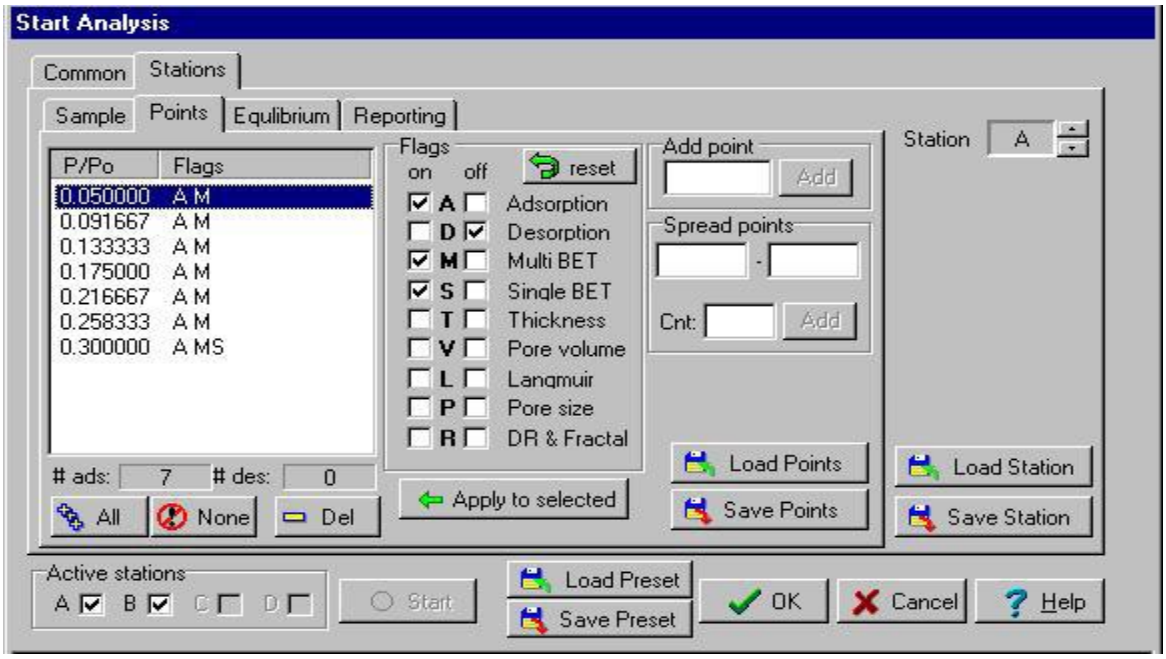

Figure 4

10. In the **Station** tab ➔ **Equilibrium** tab, leave keep the default values for pressure tolerance, equilibrium time and equilibrium timeout.
11. In the **Station** tab ➔ **Reporting** tab, choose **demo.isotherm** for autoreport option from the dropdown menu.
12. Once done with all these steps, click the **Start** button to begin the analysis.